INFLAMMATION

Hexokinase dissociation from mitochondria promotes oligomerization of VDAC that facilitates NLRP3 inflammasome assembly and activation

Sung Hoon Baik[1], V. Krishnan Ramanujan[2], Courtney Becker[1], Sarah Fett[1], David M. Underhill[1,3]*†, Andrea J. Wolf[1,3]*†

NLRP3 inflammasome activation is a highly regulated process for controlling secretion of the potent inflammatory cytokines IL-1β and IL-18 that are essential during bacterial infection, sterile inflammation, and disease, including colitis, diabetes, Alzheimer's disease, and atherosclerosis. Diverse stimuli activate the NLRP3 inflammasome, and unifying upstream signals has been challenging to identify. Here, we report that a common upstream step in NLRP3 inflammasome activation is the dissociation of the glycolytic enzyme hexokinase 2 from the voltage-dependent anion channel (VDAC) in the outer membrane of mitochondria. Hexokinase 2 dissociation from VDAC triggers activation of inositol triphosphate receptors, leading to release of calcium from the ER, which is taken up by mitochondria. This influx of calcium into mitochondria leads to oligomerization of VDAC, which is known to form a macromolecule-sized pore in the outer membranes of mitochondria that allows proteins and mitochondrial DNA (mtDNA), often associated with apoptosis and inflammation, respectively, to exit the mitochondria. We observe that VDAC oligomers aggregate with NLRP3 during initial assembly of the multiprotein oligomeric NLRP3 inflammasome complex. We also find that mtDNA is necessary for NLRP3 association with VDAC oligomers. These data, together with other recent work, help to paint a more complete picture of the pathway leading to NLRP3 inflammasome activation.

INTRODUCTION

Activation of the NOD-like receptor family pyrin domain containing 3 (NLRP3) inflammasome in macrophages to stimulate processing and secretion of the potent inflammatory cytokine interleukin-1β (IL-1β) is a key process in innate sensing of bacterial pathogens (*1*, *2*) and is a central factor in diverse inflammatory diseases, including diabetes (*3*), Alzheimer's disease (*4*, *5*), atherosclerosis (*6*), and colitis (*7*–*10*). We have previously observed that degradation of bacterial cell wall peptidoglycan (PGN) inside phagosomes is an essential step in activating the NLRP3 inflammasome after phagocytosis of Gram-positive bacteria (*11*). Further, we have observed that when bacterial cell wall PGN is degraded in phagolysosomes, large quantities of the sugar *N*-acetylglucosamine are liberated and inhibit hexokinase (HK), causing dissociation of the enzyme from outer membranes of mitochondria. We also found that dissociation of HK from mitochondria was sufficient to trigger NLRP3 inflammasome assembly and activation (*12*). However, how HK release from mitochondria subsequently triggers NLRP3 activation is not known.

NLRP3 activation involves assembly of a large oligomeric protein complex including NLRP3, apoptosis-associated speck-like protein (ASC), NIMA-related kinase 7 (NEK7), and caspase-1 (*1*, *13*). Caspase-1 is cleaved into its active form in this complex and subsequently processes proteins, including IL-1β, IL-18, and gasdermin D, into their active forms. Strong acute activation of this pathway by common experimental NLRP3 activators such as extracellular adenosine triphosphate (ATP), nigericin, or silica particles requires potassium efflux from the cytosol and results in a gasdermin-dependent inflammatory form of cell death called pyroptosis (*1*, *13*). However, not all NLRP3 activators are associated with pyroptosis or potassium efflux, and we have observed that NLRP3 activation by Gram-positive bacterial PGN does not require potassium efflux and is not associated with cell death (*12*). Similarly, Gross *et al.* (*14*) observed that small molecules that inhibit mitochondrial oxidoreductases and activate the NLRP3 inflammasome do so in a manner that does not require potassium efflux, whereas Hornung and colleagues (*15*) have noted that potassium efflux and cell death are not associated with lipopolysaccharide (LPS)–induced inflammasome activation in human monocytes. In addition, Pearlman and colleagues (*16*) have noted that activation of NLRP3 in neutrophils leads to gasdermin D activation but is not necessarily associated with cell death. Calcium movement has also been implicated in NLRP3 activation, with influx of extracellular Ca^{2+} and release of endoplasmic reticulum (ER)–linked Ca^{2+} stores being implicated (*17*). Again, different studies have come to different conclusions as to whether the role of Ca^{2+} is universally required for NLRP3 activation (*13*). Despite the extensive work done on the mechanism of NLRP3 inflammasome activation, a unifying model of upstream features of NLRP3 activation has been elusive.

Compelling evidence implicates a role for mitochondria in regulation of the NLRP3 inflammasome. Mitochondrial dysfunction (*18*), reactive oxygen, release of mitochondrial DNA (mtDNA) (*19*–*22*), exposure of cardiolipin on mitochondrial outer membranes (*23*–*25*), and viral activation of NLRP3 via sensing by mitochondrial antiviral signaling protein (MAVS) (*26*, *27*) have all been

[1]F. Widjaja Inflammatory Bowel Disease Institute, and the Karsh Division of Gastroenterology and Hepatology, Cedars-Sinai Medical Center, Los Angeles, CA 90048, USA. [2]Department of Medicine and the Department of Pathology and Laboratory Medicine, Cedars-Sinai Medical Center, Los Angeles, CA 90048, USA. [3]Department of Biomedical Sciences, Research Division of Immunology, Cedars-Sinai Medical Center, Los Angeles, CA 90048, USA.
*Corresponding author. Email: david.underhill@csmc.edu (D.M.U.); andrea.wolf@csmc.edu (A.J.W.)
†These authors contributed equally to this work.

linked to NLRP3 inflammasome activation. Further, mitochondria have been proposed as a site of initial inflammasome nucleation (*28*). Activating signals has been reported to drive relocation of NLRP3, in the cytoplasm and associated with ER membranes, to both mitochondria and mitochondria-ER contact sites called MAMs (*18*, *29*). However, the details of how this might operate are unclear.

In our previous study, we found a role for the enzyme HK in NLRP3 activation in response to bacterial PGN (*12*). HK is the first enzyme of the glycolytic pathway, and it converts glucose to glucose-6-phosphate. On the mitochondrial outer membrane, HK binds to the voltage-dependent anion channel (VDAC), a channel that, together with the adenine nucleotide translocase (ANT) in the inner mitochondrial membrane, regulates flow of metabolites, ions, and nucleotides in and out of the organelle (*30*). HK binding to VDAC is thought to provide it with preferential access to ATPs transported by VDAC and ANT out of the mitochondria. The interaction of HK with VDAC modulates cellular metabolism, with the bound form favoring oxidative phosphorylation and the released form favoring the funneling of glucose-6-phosphate more into glycolysis, leading to lactate production and the pentose phosphate pathway (*31*–*34*). Previous studies have suggested that VDAC can oligomerize in response to mitochondrial signals promoting apoptosis to allow for the formation of a multimeric structure that can allow proteins and macromolecules to escape from the mitochondria (*35*–*39*). In some cases, these oligomers interact with proteins, including Bax and Bid, to promote apoptosis (*34*, *35*, *37*, *40*). Recently, VDAC-bound HK has been noted to localize primarily to MAMs, at least in cancer cells, and HK release from these sites has been linked to increased mitochondrial Ca^{2+} caused by Ca^{2+} release from ER via inositol triphosphate receptors (IP_3Rs) and by Ca^{2+} entry through plasma membrane (*41*).

In the present study, we find that the dissociation of HK from mitochondria previously shown to be induced by PGN is also triggered, albeit by a different mechanism, by other common NLRP3 inflammasome activators, including ATP, nigericin, and silica. Release of HK allows for Ca^{2+} influx into the mitochondria and frees up VDAC to oligomerize. We find that blocking VDAC oligomerization with the inhibitor VBIT-4 reduces PGN and HK release–induced maturation and secretion of IL-1β. In agreement with recent work by Xian *et al.* (*21*), VBIT-4 also reduces maturation and secretion of IL-1β in response to ATP, nigericin, and silica, placing HK release as a common upstream factor. Knocking down any one of the three VDACs expressed by macrophages was not sufficient to inhibit inflammasome activation; however, knocking down any two reduced IL-1β secretion, suggesting that the VDACs form hetero-oligomeric structures important for NLRP3 inflammasome activation. We also find that VDAC oligomerization is followed by recruitment of NLRP3 into close association with VDAC and is accompanied by activation of inflammasomes. The association between VDAC and NLRP3 was impaired upon inhibition of VDAC oligomerization, as is IL-1β secretion. Last, we find

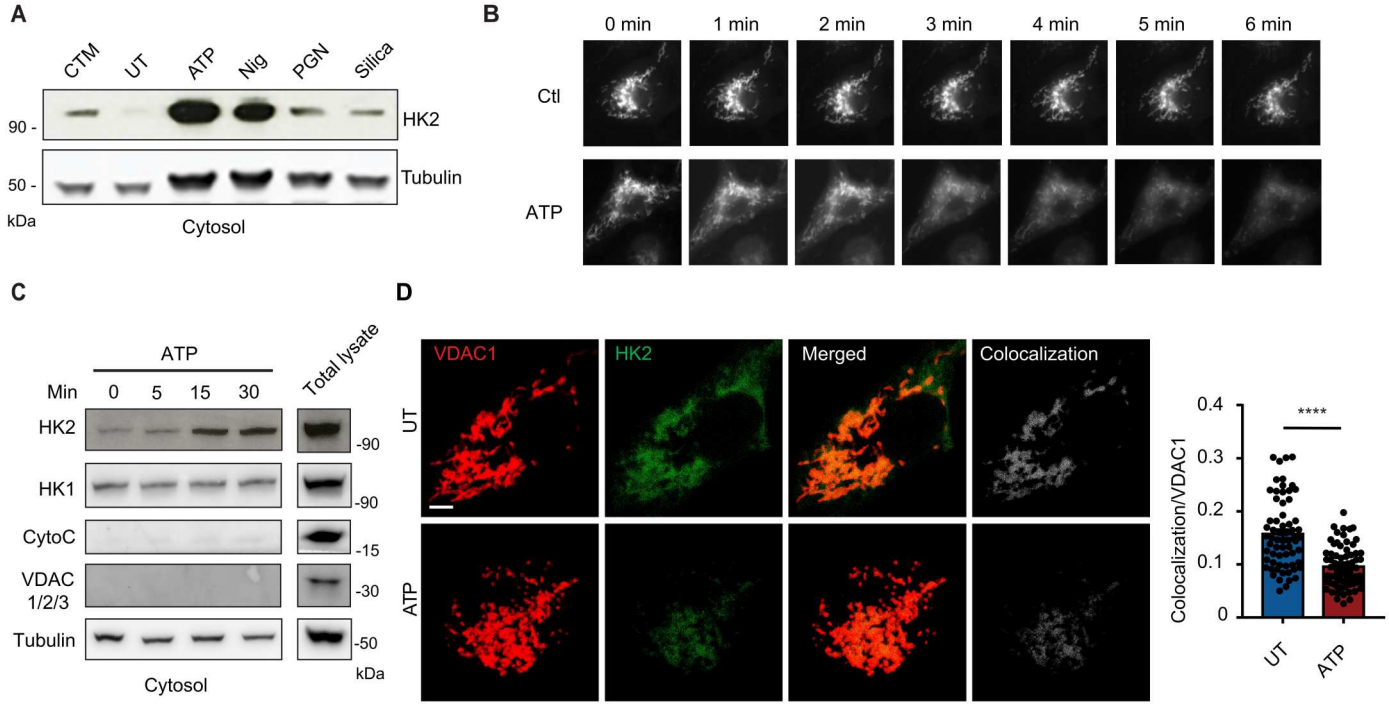

Fig. 1. Common NLRP3 inflammasome activators trigger HK release from mitochondria. (**A**) Immunoblot of HK2 and tubulin in cytosolic fractions from mouse BMDMs primed with LPS for 3 hours and left untreated (UT) or activated with ATP (5 mM; 30 min), nigericin (Nig; 3 μM; 30 min), PGN (40 μg/ml; 6 hours), or silica particles (20 μg/ml; 6 hours). Clotrimazole (CTM) treatment was used as a positive control for HK release from mitochondria. (**B**) LPS-primed BMDMs expressing HK2-GFP were imaged before and after treatment with 5 mM ATP as indicated. (**C**) Immunoblot time course of HK2 and HK1 together with controls cytochrome *c* (CytoC), VDAC 1/2/3, and tubulin in cytosol fractions from BMDMs stimulated with ATP (5 mM) for the indicated periods. (**D**) STED images of LPS-primed BMDMs costained with antibodies to VDAC1 and HK2 and stimulated or not with ATP (5 mM; 1 hour). Scale bar, 3 μm. Colocalization was quantified in multiple cells ($n = 59$ to 65 cells across five independent experiments). Data are presented as means ± SEM. ****$P < 0.0001$ (unpaired *t* test).

that mtDNA, which has previously been implicated in NLRP3 inflammasome activation, is necessary for NLRP3 association with VDAC oligomers, indicating that VDAC oligomers, together with mtDNA, collaborate to nucleate NLRP3 inflammasome assembly. Our data suggest that HK dissociation from VDAC is a proximal step in the NLRP3 inflammasome cascade, allowing for VDAC oligomerization, NLRP3 oligomerization, and inflammasome activation.

RESULTS

HK release from mitochondria is a common feature of NLRP3-inflammasome activation

As we have observed previously (*12*), when we treated mouse bone marrow–derived macrophages (BMDMs) with particulate PGN, we observed an increase in the amount of HK2 in the cytosol of the cells (Fig. 1A), consistent with its release from the mitochondrial outer membrane. We had previously observed that PGN-derived *N*-acetylglucosamine directly inhibits HK enzymatic activity, resulting in HK2 dissociation from the mitochondria, and that the ability of PGN to activate the NLRP3 inflammasome was distinct from other activators in that it did not require influx of extracellular potassium. Further, we have observed that HK dissociation from mitochondria was sufficient to trigger NLRP3 inflammasome activation (*12*). We now report that canonical NLRP3 inflammasome activators that trigger potassium influx (*42*–*44*), including ATP, nigericin, and silica particles, also drive dissociation of HK from mitochondria into the cytosol (Fig. 1A). To directly visualize this release, we expressed green fluorescent protein (GFP)–tagged HK2 in BMDMs and observed ATP-triggered release of the protein from mitochondria by live cell fluorescence imaging (Fig. 1B). Within 15 min of treatment with ATP, there is a measurable increase in HK2 in the cytosol that is not associated with a breakdown of mitochondrial structure because there is not a concurrent release of cytochrome *c* into the cytosol (Fig. 1C). Levels of HK1 in the cytosol are not affected (Fig. 1C), suggesting that this effect is specific to HK2. This may be related to the observation that HK1 has a higher affinity to VDAC1 than HK2 (*32*).

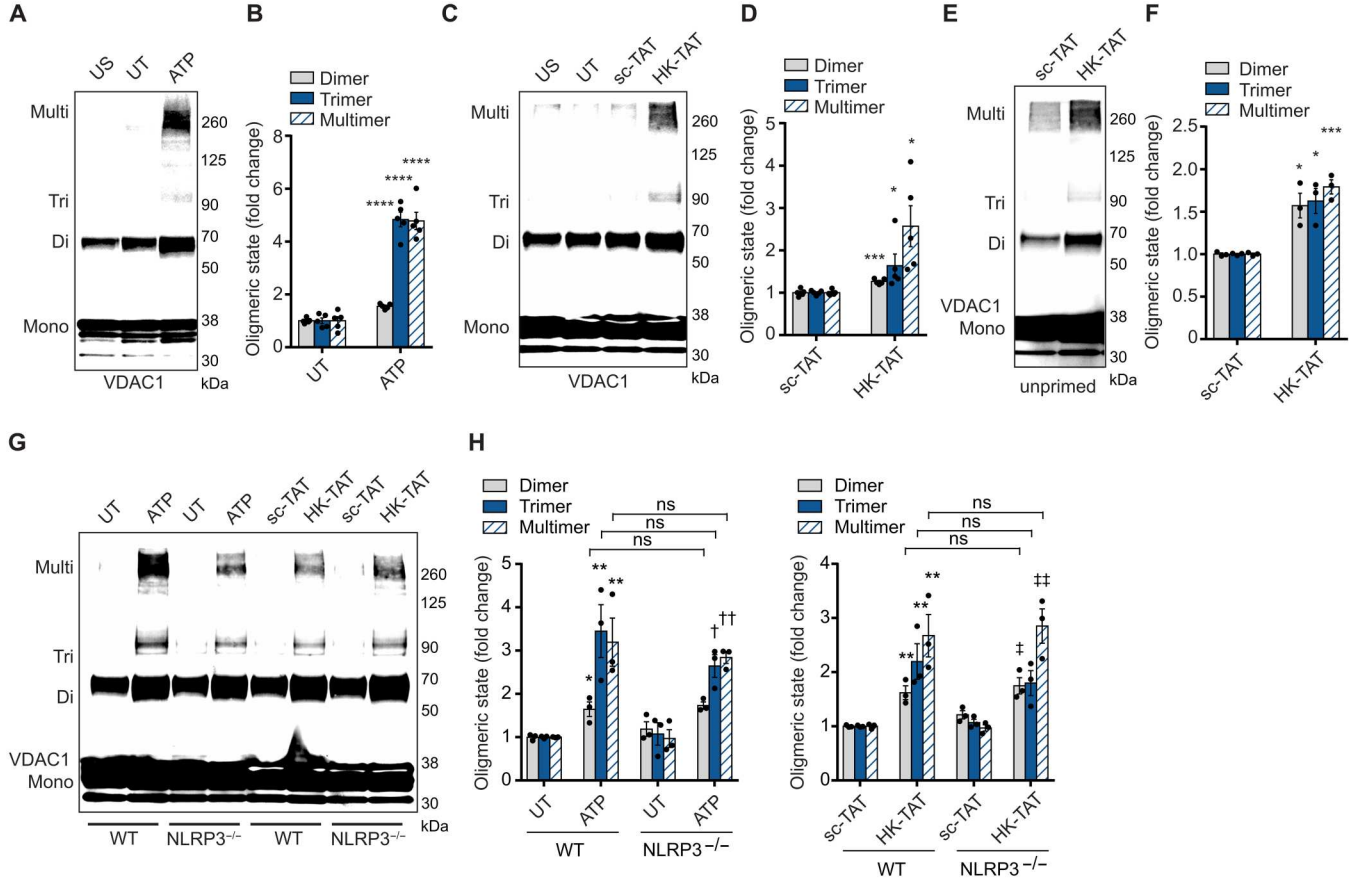

Fig. 2. NLRP3 activators trigger VDAC oligomerization. (**A** and **B**) Immunoblot of VDAC1 cross-linking in unprimed, unstimulated BMDMs (US) or LPS-primed cells left untreated (UT) or stimulated with ATP (5 mM; 1 hour) (A) and quantitative analysis of oligomers in multiple independent immunoblots (B) ($n = 5$). (**C** and **D**) Immunoblot of VDAC1 cross-linking assay as in (A) but stimulated with scramble peptide (sc-TAT) or with HK-TAT (20 μM; 2 hours) (C) and quantitative analysis of oligomers in multiple independent immunoblots (D) ($n = 5$). (**E** and **F**) Immunoblot of VDAC1 cross-linking assay as in (C) but in unprimed BMDMs (E) and quantitative analysis of oligomers in multiple independent immunoblots (F) ($n = 3$). (**G** and **H**) Immunoblot of VDAC1 cross-linking assay in LPS-primed BMDMs from wild-type (WT) or NLRP3$^{-/-}$ mice stimulated as indicated (G) and quantitative analysis of oligomers in multiple independent immunoblots (H) ($n = 3$). Graphical data are presented as means ± SEM. *$P < 0.05$, **$P < 0.01$, ***$P < 0.001$, ****$P < 0.0001$, †$p < 0.05$, ††$p < 0.01$ (compared with UT of NLRP3$^{-/-}$), ‡$p < 0.05$, and ‡‡$p < 0.01$ (compared with sc-TAT of NLRP3$^{-/-}$). ns, not significant. Comparisons were performed using unpaired *t* test (B, D, and F) or one-way ANOVA with Bonferroni correction (H).

HK2 associates with outer membranes of mitochondria through interaction of the final 15 amino acids of its N-terminal tail with VDAC1 (*34*, *35*, *45*, *46*). In resting cells, VDAC1 and HK2 colocalize by immunofluorescence microscopy (Fig. 1D), and treatment with ATP results in a marked decrease in that colocalization. Together, the data indicate that release of HK2 from the mitochondrial surface is a shared feature of common NLRP3 inflammasome activators, although the mechanisms driving that release might be different.

VDAC oligomerization is required for NLRP3 inflammasome activation

VDAC, an outer membrane channel, together with ANT in the inner mitochondrial membrane, regulates flow of metabolites, ions, and nucleotides in and out of the organelle. In some instances, particularly upon induction of apoptosis, VDAC1 has been observed to oligomerize and form a pore that can allow macromolecules through the outer mitochondrial membrane (*47*). VDAC is not absolutely necessary for formation of the permeability transition pore (PTP) that participates in collapse of mitochondria during apoptosis but may play a role in the processes (*35*, *38*, *39*, *48*, *49*). We have observed that mitochondria do not collapse upon ATP-induced HK2 release from VDAC because cytochrome *c* remains associated with the organelle (Fig. 1C), but we nevertheless examined whether ATP could allow for VDAC oligomerization. We observed by cross-linking and immunoblotting that treatment of LPS-primed BMDMs with ATP results in oligomerization of VDAC1 (Fig. 2, A and B).

To clarify whether release of HK from mitochondria is sufficient to promote VDAC oligomerization, we treated cells with HK-TAT (N-terminal HK peptide fused to transactivator of transcription peptide), a membrane-permeable form of a peptide mimicking the VDAC-binding domain of HK that has been used experimentally by us and others to specifically drive release of HK from VDAC into the cytosol and that we have found to be sufficient to trigger NLRP3 inflammasome activation in LPS-primed BMDMs (*12*, *50*, *51*). HK-TAT–induced HK dissociation from mitochondria proved to be sufficient to drive VDAC1 oligomerization (Fig. 2, C and D). A previous study has noted that VDAC oligomerization in the context of apoptotic stimuli can result from elevated expression of VDAC (*52*). We observed that treatment of cells with ATP or HK-TAT had no effect on the total cellular VDAC content (fig. S1). To better understand the placement of VDAC oligomerization in the sequence of events leading to NLRP3 inflammasome activation, we asked whether LPS priming of BMDMs was necessary for VDAC oligomerization because priming is known to prepare BMDMs by promoting expression of NLRP3 and its association with the mitochondrial outer membrane through association with cardiolipin (*23*–*25*). We observed that HK-TAT induced VDAC1 oligomerization in unprimed BMDMs (Fig. 2, E and F) and that ATP and HK-TAT induced VDAC1 oligomerization normally in NLRP3$^{-/-}$ macrophages (Fig. 2, G and H), suggesting that VDAC1 oligomerization is upstream of NLRP3 inflammasome assembly.

To determine whether VDAC oligomerization is important for NLRP3 activation as a result of HK2 dissociation from mitochondria, we made use of VBIT-4, a cell-permeable inhibitor of VDAC oligomerization (*53*–*55*). VBIT-4 blocked oligomerization of VDAC1 in ATP-stimulated BMDMs (Fig. 3, A and B). We further used nanoscale super-resolution imaging using τ-stimulated emission depletion (τ-STED) microscopy to directly observe clustering of VDAC1 on the surface of mitochondria (Fig. 3, C and D). ATP stimulated aggregation of VDAC1 into larger clusters, and this formation of larger clusters was blocked by VBIT-4, confirming that this measurement is a direct visualization of VDAC1 oligomerization. We observed that VBIT-4 blocks IL-1β production triggered by several common NLRP3 inflammasome activators in LPS-primed BMDMs (Fig. 3, E and F), but not by the AIM2 inflammasome activator poly(dA:dT) (pdA:dT) (Fig. 3E), indicating that VDAC oligomerization is specifically required for NLRP3 inflammasome activation. To confirm that the blockade of IL-1β production by VBIT-4 is due to blocking NLRP3 inflammasome activation and not some other nonspecific effect on the cells, we observed that VBIT-4 blocked release of mature processed IL-1β into the culture supernatant (Fig. 3G) and activation of caspase-1 (Fig. 3, H to J) but did not affect tumor necrosis factor–α (TNF-α) production (Fig. 3K), indicating a specific role in NLRP3 inflammasome activation. Last, VDAC oligomerization has been extensively studied in response to several apoptosis-inducing stimuli, including staurosporine (STS) (*35*, *37*, *56*), and we hypothesized that these might also therefore activate the NLRP3 inflammasome. We observed that STS triggers NLRP3-dependent IL-1β release from LPS-primed BMDMs in a manner that is inhibited by VBIT-4 (Fig. 3, L and M). Together, the data suggest that VDAC oligomerization is necessary for activation of the NLRP3 inflammasome.

Multiple VDAC proteins participate in NLRP3 activation

There are three isoforms of VDAC in mammalian cells: VDAC1, VDAC2, and VDAC3 (*57*). VDAC1 is the most abundantly expressed in most cell types, and the different VDACs have both overlapping and nonredundant functions in cells (*57*). To investigate which of the VDACs are important for NLRP3 inflammasome activation, we performed knockdown of various combinations of VDACs using clustered regularly interspaced short palindromic repeats (CRISPR) gene editing in BMDMs. We first knocked down VDAC1, VDAC3, or both in primary BMDMs and confirmed by immunoblotting that protein expression was specifically decreased by their respective target guide RNAs (gRNAs) (Fig. 4A). Knockdown of these proteins did not adversely affect LPS priming of the cells because pro–IL-1β protein was induced as well or more (Fig. 4, A and B), and TNF-α protein was produced normally (Fig. 4C). Release of IL-1β into the culture supernatant after simulation with ATP or HK-TAT was unaffected by knockdown of VDAC1 or VDAC3 alone; however, when VDAC1 and VDAC3 were suppressed together, IL-1β release was significantly reduced, suggesting overlapping roles for VDAC 1 and VDAC3 in the process (Fig. 4D). Targeted reduction of VDAC1 and/or VDAC3 had no effect on IL-1β production in response to activators of other inflammasome, including AIM2 (pdA:dT) or NLRC4 (*Salmonella*) (Fig. 4D) (*58*).

We were unable to find a good antibody to detect mouse VDAC2, so in an independent set of experiments, we knocked down VDAC2 alone or together with VDAC1 or VDAC3 and assessed mRNA knockdown by reverse transcription quantitative polymerase chain reaction (RT-qPCR) (Fig. 4E). Using LPS-primed BMDMs with each of the VDACs knocked down, we again observed that single knockdown of VDAC2 had no effect on IL-1β production stimulated by ATP but that IL-1β production was reduced when VDAC2 knockdown was combined with either VDAC1 or

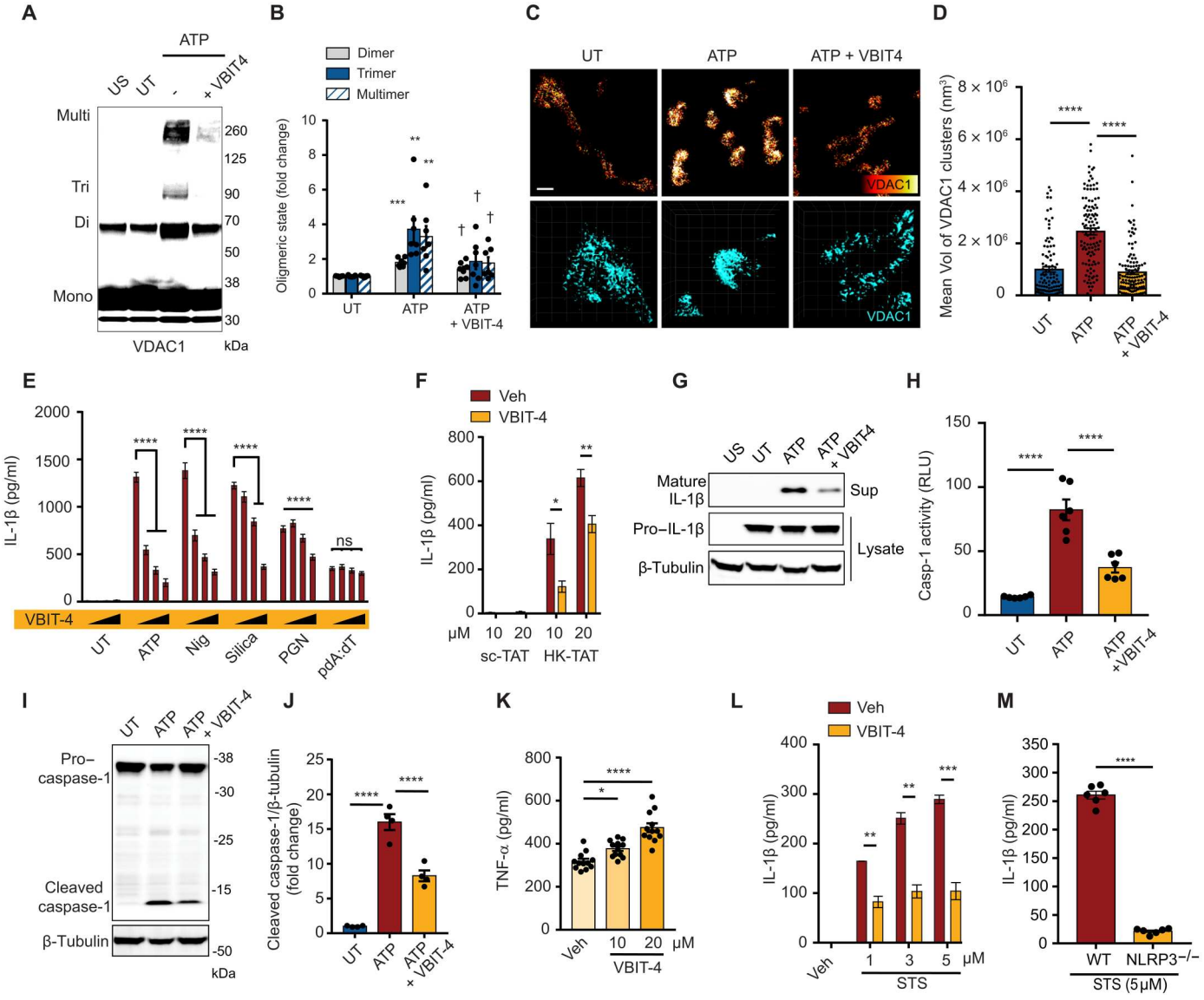

Fig. 3. VDAC oligomerization is required for NLRP3 inflammasome activation. (**A** and **B**) Immunoblot of VDAC1 cross-linking in LPS-primed BMDMs left untreated (UT) or stimulated with ATP (5 mM; 1 hour) with or without VBIT-4 (20 μM) (A) and quantitative analysis of oligomers in multiple independent immunoblots (B) ($n = 7$). (**C**) Highly magnified representative τ-STED images of VDAC1 on individual mitochondria in LPS-primed BMDMs stimulated or not with ATP (30 min) with VBIT-4 as indicated. Scale bar, 500 nm (top). Bottom: Three-dimensional images used to calculate cluster volumes (grid unit = 200 nm). (**D**) Quantification of VDAC1 cluster size derived from images as in (C) (n = 109 to 121 mitochondria across five independent experiments). (**E**) IL-1β secretion measured by ELISA from LPS-primed BMDMs stimulated as indicated [ATP (2 mM; 30 min), Nig (3 μM; 30 min), silica (20 μg/ml; 6 hours), PGN (40 μg/ml; 6 hours), or pdA:dT (1 μg/ml; 6 hours)] in the presence of increasing concentrations of VBIT-4 (5 to 20 μM) ($n = 8$ replicates across three experiments). (**F**) IL-1β secretion measured by ELISA from LPS-primed BMDMs stimulated with sc-TAT or HK-TAT (2 hours) at the indicated concentrations in the presence of absence of VBIT-4 ($n = 6$). (**G** to **J**) LPS-primed BMDMs were stimulated or not with ATP in the presence or absence of VBIT-4 as in (E). The presence of mature IL-1β in culture supernatants and pro–IL-1β in cell lysate was assessed by immunoblotting (G), activation of caspase-1 was assessed in cell pellets ($n = 6$) (H), and cleaved caspase-1 in cell lysates was detected by immunoblotting (I) and quantified across multiple independent immunoblots (J) ($n = 4$). (**K**) BMDMs were primed with LPS in the presence or absence of VBIT-4, and TNF-α production was assessed by ELISA ($n = 12$ across three experiments). (**L**) LPS-primed BMDMs were treated with STS (5 μM; 6 hours) in the presence or absence of VBIT-4, and IL-1β production was assessed by ELISA ($n = 3$). (**M**) IL-1β was measured in LPS-primed WT or NLRP3$^{-/-}$ BMDMs treated with STS, and IL-1β production was assessed by ELISA ($n = 6$). Data are presented as means ± SEM. $^{*}P < 0.05$, $^{**}P < 0.01$, $^{***}P < 0.001$, $^{****}P < 0.0001$ (compared with UT if not otherwise indicated), and $^{\dagger}P < 0.05$ (compared with ATP). Comparisons were performed by one-way ANOVA withTukey's post hoc test (B, D, E, H, J, and K) or unpaired t test (F, L, and M).

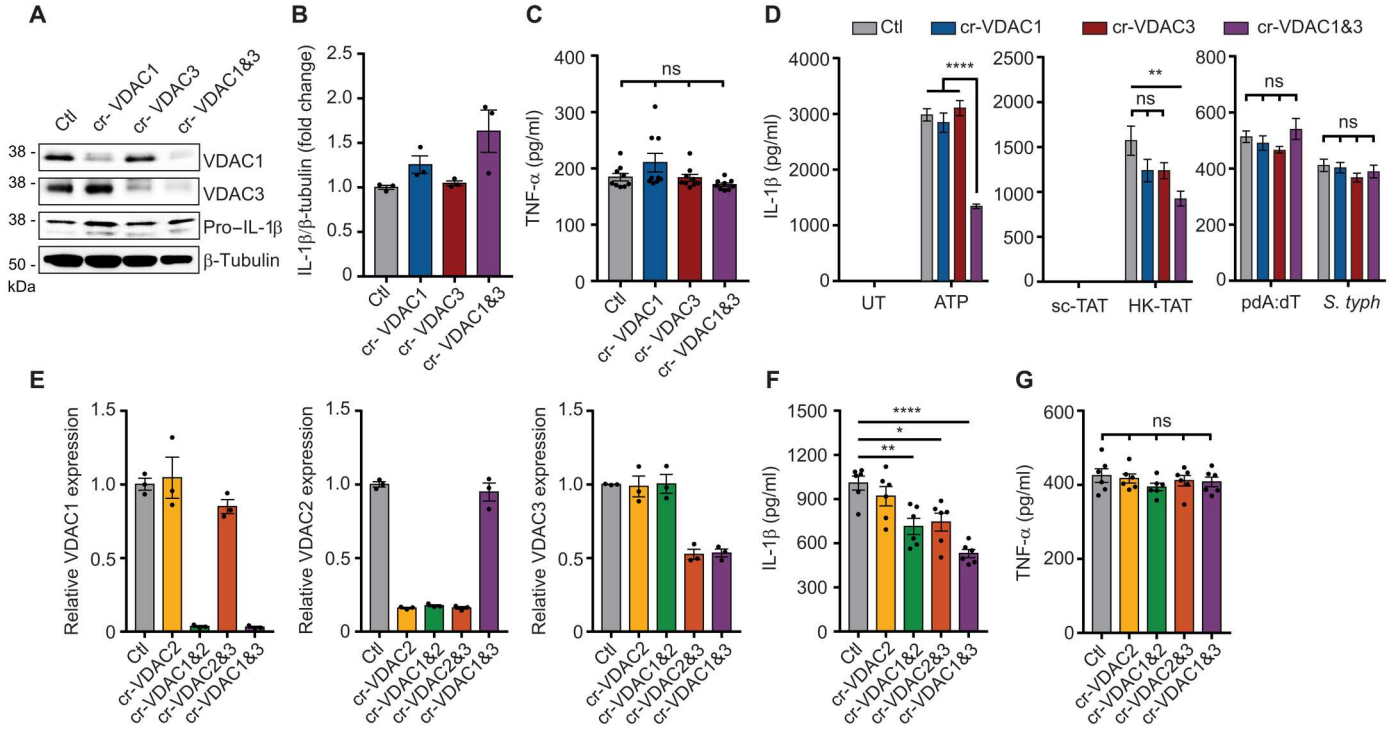

Fig. 4. Multiple VDACs participate in NLRP3 inflammasome activation. (**A**) Immunoblot of VDAC1, VDAC3, IL-1β, and β-tubulin from LPS-primed BMDMs in which VDAC1 and/or VDAC3 were knocked down using gRNAs (cr-VDAC1, cr-VDAC3, and Ctl = control/no gRNA). (**B**) Combined quantitative analysis of pro–IL-1β protein expression across independent experiments ($n = 3$). (**C**) Secretion of TNF-α into the culture supernatant was measured by ELISA ($n = 9$ replicates across three experiments). (**D**) IL-1β secretion was measured by ELISA in culture supernatants of LPS-primed cells with ATP ($n = 11$ replicates across three experiments), HK-TAT ($n = 6$ replicates across two experiments), pdA:dT or infection with *S. typhimurium* ($n = 12$ replicates across three experiments). (**E**) Relative mRNA expression of VDAC1, VDAC2, and VDAC3 was measured by RT-qPCR in BMDMs in which VDACs were knocked down as indicated ($n = 3$ biological replicates). (**F**) IL-1β secretion was measured by ELISA from primed BMDMs with the indicated VDACs knocked down and induced with ATP ($n = 6$). (**G**) TNF-α secretion in primed BMDMs in which the indicated VDACs were knocked down ($n = 6$). Data are presented as means ± SEM. $^*P < 0.05$, $^{**}P < 0.01$, $^{***}P < 0.001$, and $^{****}P < 0.0001$ (one-way ANOVA, Tukey's post hoc test).

VDAC3 (Fig. 4F). Again, no combination of VDAC knockdown affected TNF-α production (Fig. 4G). Together, the data suggest that all three forms of VDAC can influence NLRP3 activation in primary macrophages.

HK dissociation from mitochondria activates release of ER calcium

It has previously been noted in HeLa cells that the HK2/VDAC complex is associated with IP_3Rs in ER membranes at sites where the ER and mitochondria are closely associated and that dissociation of HK2 from mitochondria activates IP_3Rs (*41*). IP_3Rs regulate release of calcium from ER stores, and we therefore wondered whether this calcium release could be responsible for VDAC oligomerization in response to NLRP3 activators. We observed that an inhibitor of IP_3Rs, 2-aminoethoxydiphenyl borate (2-APB), blocks IL-1β secretion from LPS-primed BMDMs activated with either ATP or HK-TAT (Fig. 5A) and that HK2 dissociation from mitochondria induced by HK-TAT is sufficient to trigger an elevation of mitochondrial calcium concentrations in LPS-primed BMDMs that is inhibited by 2-APB (Fig. 5B). Calcium entry into mitochondria was not a consequence of NLRP3 activation because both ATP and HK-TAT induced mitochondrial calcium elevation in NLRP3-deficient macrophages (fig. S2, A and B). Calcium may enter mitochondria through the calcium uniporter on the inner mitochondrial membrane, which is inhibited by ruthenium red (RuR) (*59*, *60*). RuR has also been implicated in direct binding to VDAC to regulate Ca^{2+} movement across the outer membrane (*61*). We observed that RuR inhibited ATP and HK-TAT–stimulated IL-1β production from LPS-primed BMDMs (Fig. 5C) and inhibited the elevation of mitochondrial calcium levels in response to these stimuli (Fig. 5, D and E). These data suggest that IP_3R-triggered calcium elevation may be required for VDAC oligomerization, and we found that VDAC oligomerization triggered by ATP or HK-TAT is blocked by 2-APB (Fig. 5, F and G). Last, cyclophilin D has been identified as a key regulator of oligomerization of VDAC and ANT in formation of the PTP in response to changes in the mitochondrial environment (*62*). Cyclophilin D is inhibited by cyclosporin A (CsA), and others have noted that CsA inhibits NLRP3 inflammasome activation by canonical NLRP3 activators, although the exact mechanism of this has not been clear (*19*, *21*). We found that CsA also blocks inflammasome activation and IL-1β secretion in response to HK2 release from mitochondria induced by HK-TAT (fig. S2C).

Calcium flow from the ER to mitochondria is thought to be facilitated by a protein complex containing VDAC, IP_3R, and glucose-regulated protein 75 (GRP75; product of *Hspa9*), and depletion of GRP75 was found to interfere with calcium transfer to mitochondria (*63*, *64*). We therefore investigated whether calcium influx into

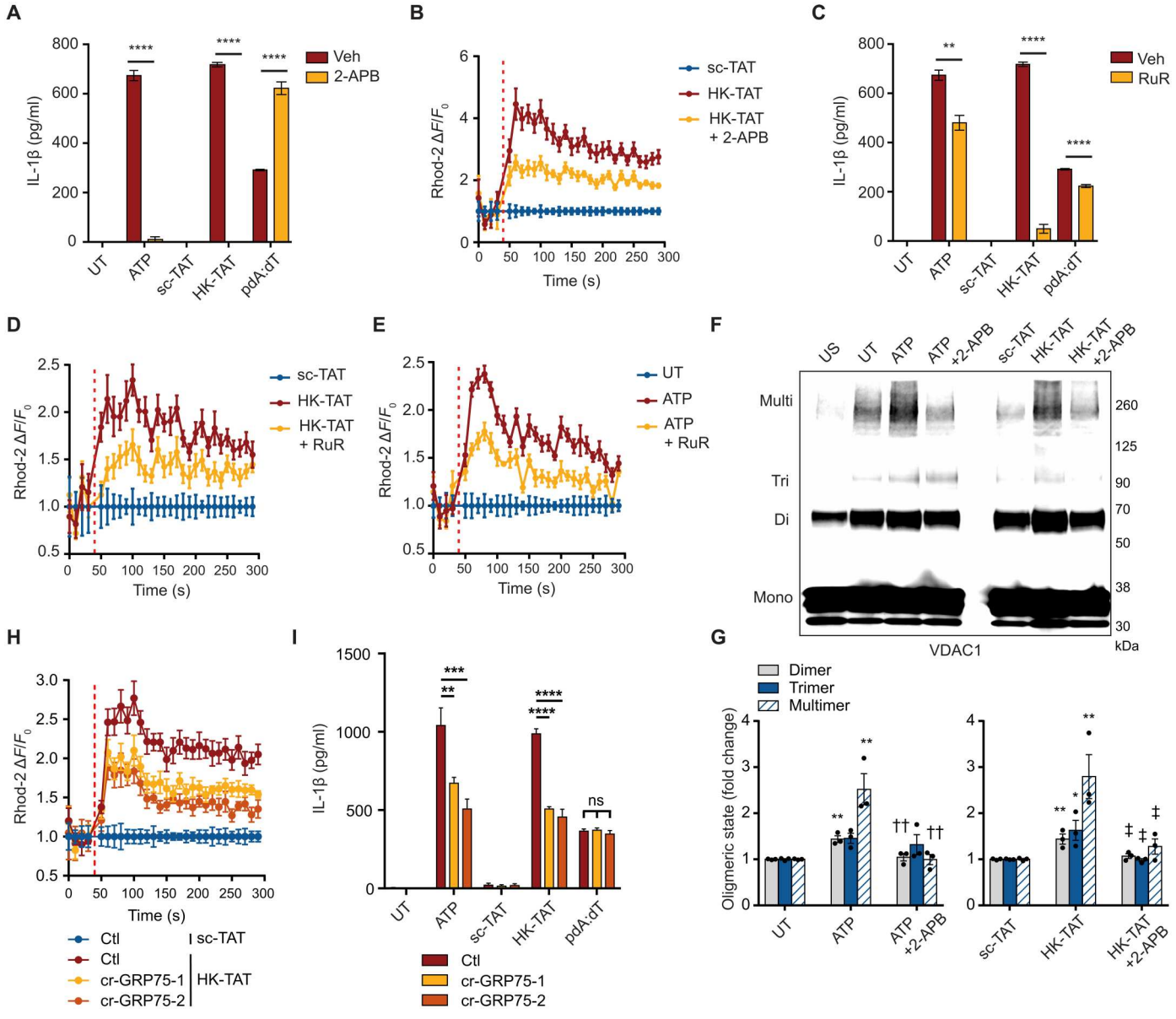

Fig. 5. ER calcium stores drive VDAC oligomerization. (**A**) LPS-primed BMDMs were stimulated or not (Veh, vehicle control) in the presence or absence of the IP_3R antagonist 2-APB (100 μM), and IL-1β production was assessed by ELISA ($n = 3$). (**B**) Primed cells were stimulated with HK-TAT in the presence or absence of 2-APB, and mitochondrial Ca^{2+} levels were assessed by Rhod-2 fluorescence over time ($n = 6$). (**C**) IL-1β was measured as in (A) but in the presence or absence of RuR (30 μM) ($n = 3$). (**D** and **E**) Ca^{2+} was measured as in (B) but in cells stimulated with HK-TAT (D) or ATP (E) in the presence or absence of RuR ($n = 6$). (**F** and **G**) BMDMs were left unprimed (US) or LPS-primed and treated (ATP, HK-TAT) or not (UT) in the presence or absence of 2-APB as indicated, and oligomerization of VDAC1 was assessed by immunoblot (F) and quantitative analysis of oligomers in multiple independent immunoblots (G) ($n = 3$). (**H**) Mitochondrial Ca^{2+} was measured as in (B) in HK-TAT–stimulated cells in which GRP75 was knocked down using two different gRNAs (cr-GRP75-1 and cr-GRP75-2) ($n = 6$). (**I**) IL-1β was measured as in (A) in cells in which GRP75 was knocked down ($n = 6$). Data are presented as means ± SEM. $^*P < 0.05$, $^{**}P < 0.01$, $^{***}P < 0.001$, $^{****}P < 0.0001$, $^{\dagger}P < 0.05$ (compared with ATP), and $^{\ddagger}P < 0.05$ (compared with HK-TAT). Comparisons were performed by unpaired *t* test (A and C) or one-way ANOVA with Bonferroni correction (G and I).

mitochondria induced by HK release from mitochondria was dependent on GRP75. CRISPR-Cas9 knockdown of GRP75 in BMDMs (fig. S2D) suppressed calcium influx into mitochondria induced by HK-TAT (Fig. 5H) and stimulation of secretion of IL-1β (Fig. 5I). Together, the data suggest that when NLRP3 activators trigger HK2 dissociation from mitochondria, this causes ER calcium stores to be released by IP_3Rs, and the subsequent elevation of mitochondrial calcium levels triggers VDAC oligomerization.

To understand whether these observations linking calcium influx–triggered oligomerization of VDAC are consistent for stimuli that trigger NLRP3 activation in distinct ways, we first investigated noncanonical activation via caspase-11 (*15*, *65*, *66*). We observed that IL-1β production in response to transfection with LPS was inhibited by VBIT-4 and 2-APB (fig. S3A), but there is only a partial impact on cytotoxicity induced by transfected LPS (fig. S3B). These data are consistent with the cytotoxicity being driven by

initial caspase-11 gasdermin D cleavage that feeds into NLRP3/caspase-1 activation and IL-1β production (*65*, *66*). We also examined the effects on NLRP3 activation downstream of imiquimod and CL097, which have been reported to activate NLRP3 independent of potassium efflux (*67*). We observed that IL-1β production in response to both stimuli was inhibited by VBIT-4 and 2-APB (fig. S3, C and D). We also investigated alternative NLRP3 activation upon treatment of human monocytes with LPS and observed that both VBIT-4 and 2-APB inhibited IL-1β produced by LPS-stimulated human monocytes (fig. S3E). These data imply that even when NLRP3 is activated by alternative or noncanonical stimuli, there is still a role for VDAC oligomerization and mitochondrial Ca^{2+} uptake.

VDAC oligomers directly recruit NLRP3

We next wondered how VDAC oligomerization might be mechanistically linked to NLRP3-driven assembly of inflammasomes. Because inflammasome assembly is an oligomerization process itself, we hypothesized that VDAC oligomerization might be harnessed to promote assembly of the NLRP3 inflammasome or that the oligomerized structure of VDAC might facilitate direct interaction with NLRP3. NLRP3 has been previously described to be associated with mitochondria (*18*, *23*, *68*, *69*), and we therefore explored whether NLRP3 might directly interact with VDAC. Using a proximity ligation assay, we found that VDAC1 and VDAC3 are not in close proximity with NLRP3 in resting cells (Fig. 6, A and C), but the VDACs come into close proximity with NLRP3 upon stimulation of VDAC oligomerization with HK-TAT (Fig. 6, A to D). Association of NLRP3 with VDAC1 is also induced by ATP, and NLRP3 recruitment requires VDAC oligomerization because the association is inhibited by VBIT-4 (Fig. 6, E and F). The specificity of the VDAC1-NLRP3 proximity ligation signal was confirmed by the loss of ATP-induced proximity ligation signal in NLRP3-deficient cells (fig. S4A). We observed that VDAC oligomerization drives relatively large-scale recruitment of NLRP3 by simple colocalization using τ-STED–fluorescence lifetime imaging (FLIM), which has a spatial resolution of around 60 nm. Whereas some colocalization of VDAC1 and NLRP3 is observed in resting cells, this colocalization is markedly elevated upon stimulation of oligomerization with ATP (Fig. 6, G and H). This colocalization is reduced to resting levels by blocking VDAC oligomerization with VBIT-4. ATP-induced colocalization was also lost in NLRP3-deficient cells, confirming the specificity of the assay (fig. S4, B and C). We further independently confirmed the close association of VDAC1 and NLRP3 using fluorescence acceptor photobleaching. In resting cells, there is a modest amount of fluorescence resonance energy transfer (FRET) between antibody-labeled VDAC1 and NLRP3, but the efficiency of the FRET increases markedly upon stimulation of VDAC oligomerization with ATP (Fig. 6, I and J). The increased FRET is due to VDAC oligomerization because it is inhibited by VBIT-4. As an independent way to inhibit VDAC oligomerization, we treated cells with the IP_3R inhibitor 2-APB, which blocks VDAC oligomerization (Fig. 5F) and found that 2-APB also blocked VDAC association with NLRP3 as measured by proximity ligation (Fig. 6, K and L). Inhibition of NLRP3 association with VDAC by 2-APB was not due to a block in NLRP3 localization to the mitochondria because isolation of mitochondria revealed an equal amount of NLRP3 bound in HK-TAT–treated cells with or without 2-APB treatment (Fig. 6M). These results confirm previous observations that NLRP3 is recruited to mitochondria after LPS priming and before NLRP3 inflammasome activation (*23*, *69*) and add that NLRP3 only associates with VDAC when VDAC oligomerizes.

mtDNA is necessary for NLRP3/VDAC aggregation

Last, many investigators have noted that oxidized mtDNA can leak out of mitochondria during inflammasome activation and that this mtDNA is important for activation of the NLRP3 inflammasome (*19*–*22*, *70*). We therefore wondered what role mtDNA might have when VDAC oligomerization is induced by HK release. mtDNA can be depleted from cells by culturing in the presence of ethidium bromide (EtBr) (*21*, *22*, *71*). We therefore cultured cells with EtBr and confirmed depletion of mtDNA by qPCR (Fig. 7A). As expected, IL-1β production triggered by NLRP3 activators that drive HK release from mitochondria and VDAC oligomerization, including ATP, PGN, silica, and HK-TAT, was reduced in cells depleted of mtDNA (Fig. 7B). However, VDAC oligomerization occurred normally in cells depleted of mtDNA (Fig. 7, C and D), placing VDAC oligomerization upstream of a role for mtDNA in NLRP3 inflammasome activation. However, NLRP3 recruitment to VDAC oligomers, as measured by proximity ligation assay, was blocked in cells depleted of mtDNA by EtBr but does not require ASC (Fig. 7, E and F). Association of NLRP3 with mitochondria increased with priming as seen previously (*23*), but in LPS-primed cells depleted of mtDNA, there was no effect on NLRP3 recruitment to mitochondria (Fig. 7G).

To better understand the role of mtDNA in assembly of the NLRP3-VDAC complex, we tested whether delivery of mtDNA into the cytosol would be sufficient to drive the association. In wild-type cells, transfection of mtDNA induced production of IL-1β in an AIM2-dependent manner (fig. S5) consistent with previous studies (*72*). Therefore, to further understand the role of mtDNA in NLRP3 inflammasome activation, we performed experiments in $AIM2^{-/-}$ BMDMs. Transfection of mtDNA into LPS-primed $AIM2^{-/-}$ BMDMs is not sufficient to drive IL-1β production (Fig. 7H and fig. S5), nor can mtDNA alone drive VDAC1-NLRP3 association (Fig. 7, I and J). However, in $AIM2^{-/-}$ BMDMs that have been depleted of their endogenous mtDNA with EtBr, transfection of exogenous mtDNA enhanced IL-1β production (Fig. 7H) and restored VDAC1-NLRP3 association (Fig. 7, I and J) that was normally lost in mtDNA-depleted cells (Fig. 7, E and F). Together, the data suggest that NLRP3 is poised for inflammasome activation by associating with mitochondria but that VDAC oligomerization drives assembly of a larger NLRP3 complex and leads to inflammasome activation. In addition, the NLRP3 recruitment to VDAC oligomers requires mtDNA.

DISCUSSION

The NLRP3 inflammasome is a signaling complex central to inflammation in defense against microbial infection and in sterile inflammation and multiple disease processes, including atherosclerosis, myocardial infarction, steatohepatitis, and colitis, among others (*1*, *13*). Considerable progress has been made in mapping out the molecular signals and mechanisms that coordinate activation and assembly of this large multiprotein complex. However, given the diverse range of stimuli and signaling pathways that have been reported to trigger or influence NLRP3 inflammasome assembly, unifying factors controlling initial recruitment and assembly of the

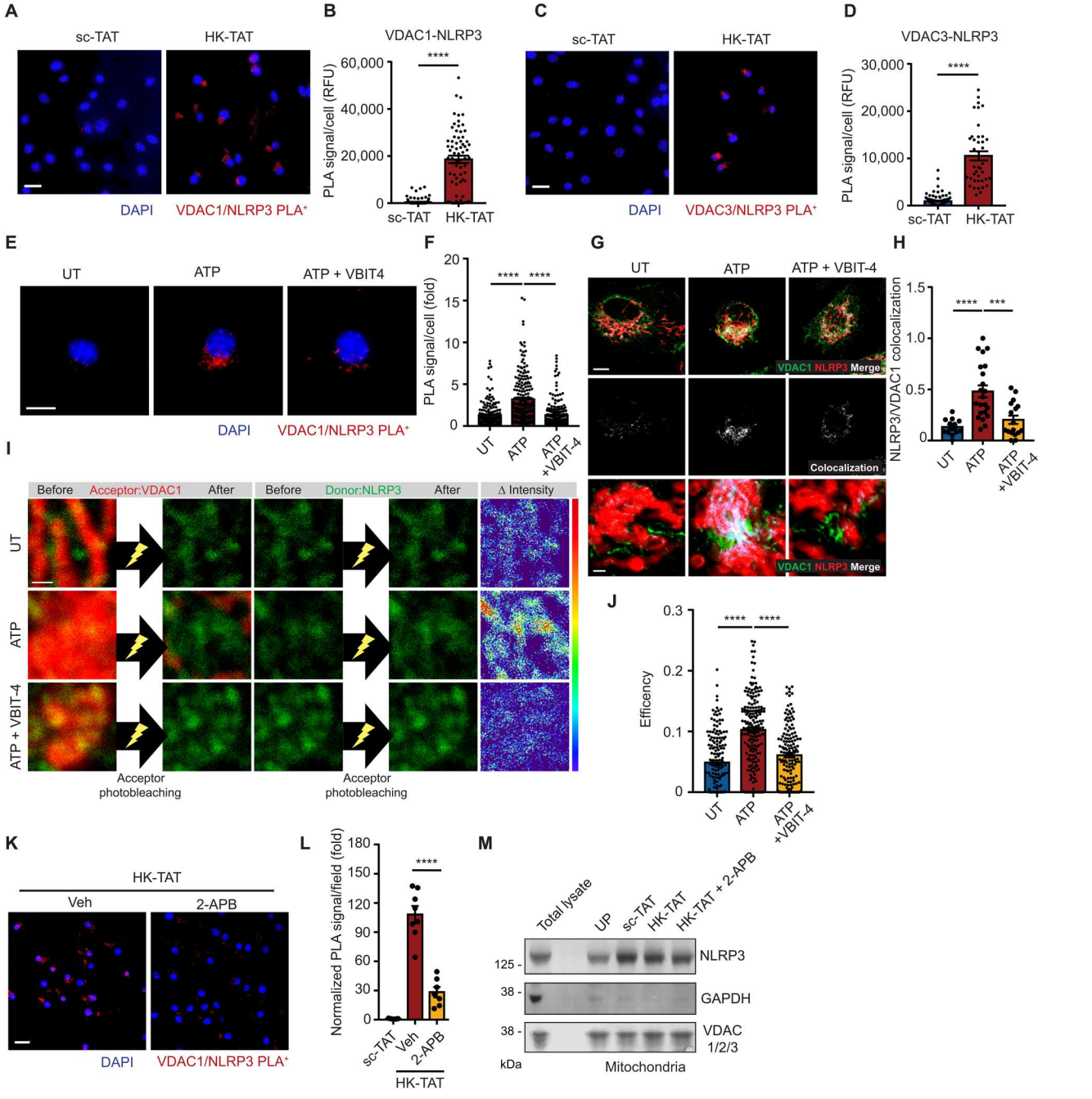

Fig. 6. VDAC oligomers associate with NLRP3 during inflammasome activation. (**A** and **B**) LPS-primed BMDMs were stimulated with sc-TAT or HK-TAT (20 μM; 2 hours), and close association between VDAC1 and NLRP3 was assessed by proximity ligation assay (A) (scale bar, 20 μm) and quantified (B) (n = 70 to 102 cells across three independent experiments). RFU, relative fluorescence units. (**C** and **D**) VDAC3-NLRP3 close association was assessed as in (A and B) (n = 42 to 109 cells across three independent experiments). (**E** and **F**) VDAC1-NLRP3 close association was assessed as in (A) and (B) (E) (scale bar, 10 μm), except that cells were stimulated or not with ATP (2 mM; 30 min) (n = 162 to 236 cells across five independent experiments). (**G** and **H**) τ-STED–FLIM images of individual UT or ATP-treated BMDMs (2 mM; 30 min) with or without VBIT-4 (20 μM; 1 hour) using antibodies against VDAC1 and NLRP3 (top row; scale bar, 5 μm), and colocalization between VDAC1 and NLRP3 is highlighted (middle row). More magnified regions (bottom row) highlight areas of colocalization (scale bar, 0.5 μm). Colocalization was quantified (H) (n = 13 to 22 cells across three independent experiments). (**I** and **J**) Acceptor photobleaching assay with UT or ATP-treated BMDMs with or without VBIT-4 using antibodies against VDAC1 as the acceptor (red) and NLRP3 as a donor (green). Representative images (I) of VDAC1 and NLRP3 before and after acceptor photobleaching (left and middle; scale bar, 0.5 μm) and the amounts of changes of the intensity of donor shown by RGB spectrum (right). The degree of acceptor photobleaching was quantified (J) (n = 150 to 181 photobleached areas from 16 cells across three experiments). (**K** and **L**) VDAC1-NLRP3 close association was assessed as in (A) and (B) in cells treated or not with the IP_3R inhibitor 2-APB (n = 5 to 8 imaged areas normalized by DAPI count across two independent experiments) (scale bar, 20 μm). (**M**) Mitochondrial fractions from unprimed (UP) BMDMs or from LPS-primed BMDMs stimulated as indicated were assessed for the presence of NLRP3, VDAC1, and GAPDH by immunoblotting. A total lysate was included for antibody reference. Data are presented as means ± SEM. (F, J, and L) ***P < 0.001 and ****P < 0.0001 (one-way ANOVA, Tukey's post hoc test). (B and D) ****P < 0.0001 (unpaired t test).

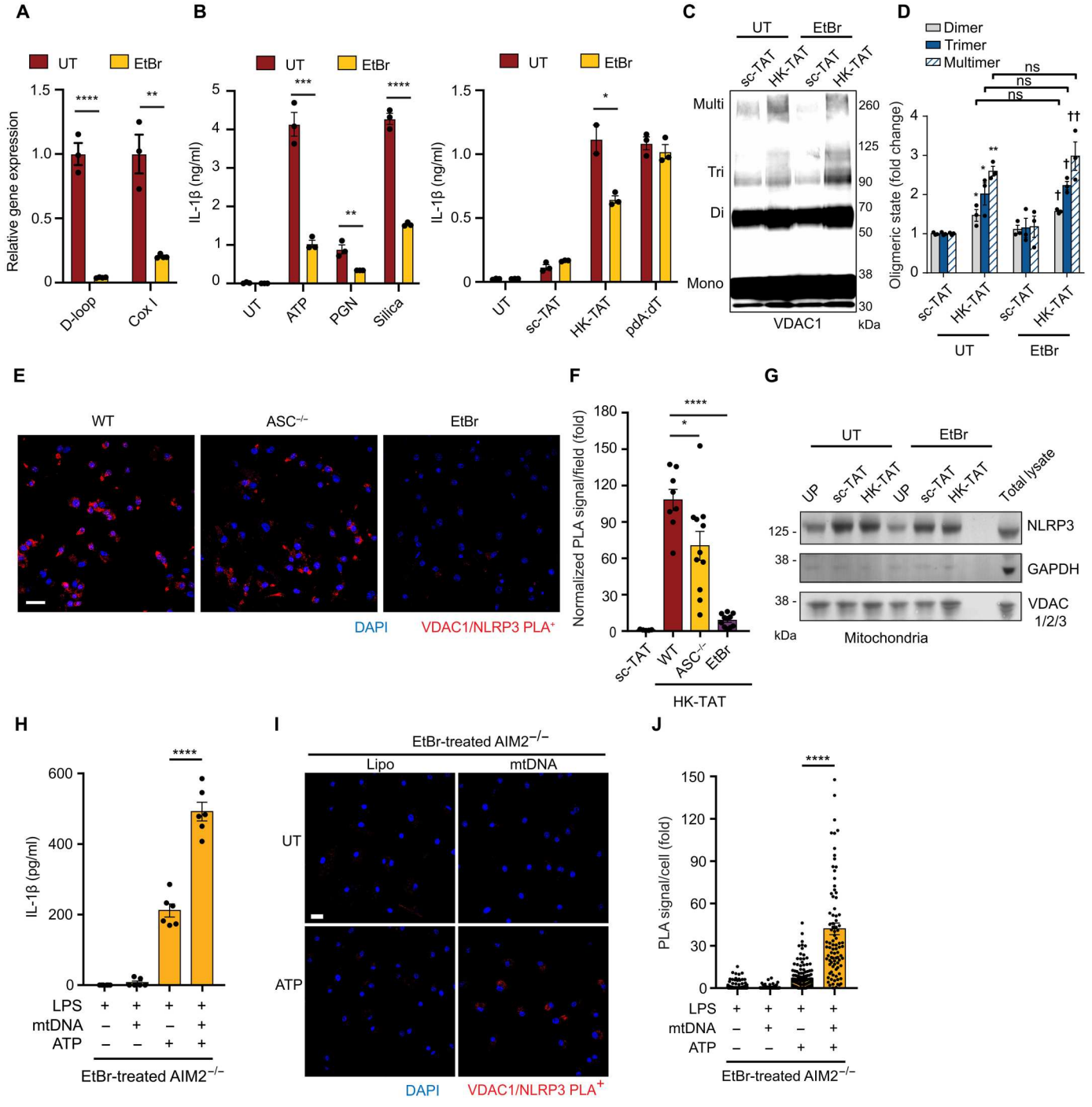

Fig. 7. mtDNA promotes NLRP3 association with VDAC oligomers. (**A**) BMDMs were grown in the presence of EtBr to deplete mtDNA, and depletion was confirmed by quantitative PCR of two regions of mtDNA (D loop and CoxI) normalized to nuclear DNA ($n = 3$). (**B**) EtBr-treated BMDMs were LPS-primed and stimulated with ATP (5 mM; 2 hours), PGN (40 μg/ml; 6 hours), silica (20 μg/ml; 6 hours), or sc-TAT and HK-TAT (20 μM; 2 hours), or pdA:dT (1 μg/ml; 6 hours), and IL-1β was measured by ELISA ($n = 3$). (**C** and **D**) BMDMs treated or not with EtBr were LPS-primed and treated with sc-TAT or HK-TAT. Oligomerization of VDAC1 was assessed by immunoblot (C) and quantitative analysis of oligomers in multiple independent immunoblots (D) ($n = 3$). (**E** and **F**) LPS-primed WT, ASC$^{-/-}$, or EtBr-treated BMDMs were stimulated with HK-TAT, and close association between VDAC1 and NLRP3 was assessed by proximity ligation assay (E) (scale bar, 20 μm) and quantified (F) ($n = 5$ to 11 imaged areas normalized by DAPI count across two independent experiments). (**G**) NLRP3, GAPDH, and VDAC levels were assessed by immunoblotting of mitochondrial fractions from BMDMs and EtBr-treated BMDMs primed with LPS and stimulated as indicated or left unprimed (UP). (**H**) IL-1β was measured in EtBr-treated AIM2$^{-/-}$ BMDMs primed with LPS and stimulated with or without mtDNA or ATP ($n = 6$). (**I** and **J**) LPS-primed EtBr-treated AIM2$^{-/-}$ BMDMs were stimulated or not with ATP, and close association between VDAC1 and NLRP3 was assessed by proximity ligation assay (I) (scale bar, 20 μm) and quantified (J) ($n = 90$ to 176 cells across three independent experiments). Data are presented as means ± SEM. *$P < 0.05$, **$P < 0.01$, ***$P < 0.001$, ****$P < 0.0001$, and †$P < 0.05$ (compared with sc-TAT of EtBr-treated BMDMs). Comparisons were made by unpaired *t* test (A, B, and F) or one-way ANOVA with Bonferroni correction (D) or Tukey's post hoc test (H and J).

complex have been especially challenging to identify. In this study, we find that a common step in NLRP3 inflammasome activation is the dissociation of HK2 from the outer mitochondrial membrane channel VDAC (fig. S6). HK dissociation from mitochondria activates IP_3R signaling, initiating the release of calcium from the ER that flows into mitochondria. The data suggest that elevated matrix calcium drives oligomerization of VDAC on the outer membrane that, together with inner membrane partners, forms pores, which is consistent with previous observations about VDAC oligomerization (*47*). This oligomerized VDAC, together with mtDNA fragments that have access to the outside of the mitochondria, perhaps through the open pore, recruits NLRP3 to a VDAC-NLRP3 complex on the mitochondrial surface that is important for assembly of the active NLRP3 inflammasome (fig. S6).

Mechanistically, the HK2/VDAC complex has been shown to localize to regions where mitochondria and ER membranes are tightly associated and interact directly with ER IP_3Rs (*41*), and, consistent with our observations in macrophages, dissociation of HK from this complex has been observed to be sufficient to activate IP_3R-mediated calcium release and has been reported to contribute to altered VDAC conductance (*45*). In addition, GRP75 has been implicated in coupling ER IP_3Rs to VDAC and facilitating calcium flow from ER stores into mitochondria (*63*, *64*). Consistent with this, we find that GRP75 is required for elevation of mitochondrial calcium levels triggered by HK release. Elevated matrix calcium has been well characterized as a regulator of activation of the "mitochondria PTP," an activity that is regulated by cyclophilin D, although the role of VDACs in this complex, once considered certain, is currently less clear (*73*). The mitochondrial PTP is a still incompletely characterized assembly of inner and outer membrane mitochondrial proteins that allow flow of low–molecular weight solutes, including fragments of mtDNA, across the normally impermeable inner membrane. VDACs may function as a part of the pore or as regulators and associated proteins. Nevertheless, we observe that IP_3R-regulated Ca^{2+} flux drives oligomerization of VDAC on the mitochondrial surface in response to HK dissociation.

The Shoshan-Barmatz laboratory (*47*) has done extensive work reporting that VDAC has the ability to oligomerize and generate a macromolecule-sized pore in the outer membranes of mitochondria that can pass mtDNA fragments (*47*). They observed in mouse embryo fibroblasts that short mtDNA fragments could cross mitochondrial membranes via oligomerized VDAC1 channels and were released into the cytosol, where they triggered type I interferon signaling, and that VBIT-4 can inhibit this process (*55*). These data, together with the data presented here, are consistent with recent data from Xian *et al.* (*21*), who found in macrophages that mtDNA release and subsequent type I interferon signaling in response to inflammasome activators are blocked by VBIT-4. In addition, consistent with our findings, Xian *et al.* (*21*) noted that VBIT-4 inhibits NLRP3 inflammasome activation by canonical stimuli. Kim *et al.* (*55*) observed that mtDNA binds directly to VDAC1 and promotes oligomerization of purified VDAC1, suggesting that production of mtDNA fragments itself might promote formation of VDAC1 oligomers. In contrast, both Xian *et al.* (*21*) and our data suggest that depletion of mtDNA in macrophages does not reduce VDAC oligomerization in response to NLRP3 activators, pointing at other upstream activators of VDAC oligomerization. Our data suggest that release of HK from VDAC in macrophages, together with the resulting IP_3R-mediated Ca^{2+} elevation in mitochondria, promotes the VDAC oligomerization (*48*).

Somewhat divergent from previous observations about the role of the three VDACs in NLRP3 inflammasome activation (*18*, *21*), where individual knockdown of individual VDACs was sufficient to inhibit the NLRP3 inflammasome, we find that knockdown of one VDAC is not sufficient to block NLRP3 inflammasome activation. One possible explanation for the different data is likely a differential level of VDAC knockdown between experiments. We interpret the data to suggest that the overall amount of the three VDACs is what is important. However, previous studies did not perform combination knockdown of the VDACs, and our data clearly indicate that combined knockdown of any two VDAC affected NLRP3 activation. Unlike previous studies, our knockdown data, as well as data showing NLRP3 and VDAC3 in close association, indicate that the different VDAC isoforms collaborate in influencing NLRP3 activation.

Shimada *et al.* (*19*) initially observed that oxidized mtDNA was produced by cells stimulated with NLRP3 inflammasome activators and that oxidized mtDNA fragments directly interact with NLRP3. Several studies have since reported that LPS priming leads to increased production of mtDNA fragments and that alterations in mitochondrial endonucleases and DNA repair machinery affect mtDNA production and NLRP3 inflammasome activation (*19*–*21*). Thus far, the data support a model in which mtDNA needs to exit the mitochondria across both mitochondrial membranes to have an inflammatory impact. Experiments using the PTP inhibitor CsA implicate cyclophilin D and PTP in mtDNA crossing the inner mitochondrial membrane (*19*–*22*, *70*). Here, we report together with recent work (*21*) that VDAC can oligomerize to form a macromolecule-sized pore allowing for mtDNA to transit the outer mitochondrial membrane. Because it has been reported that mtDNA can also bind to VDAC directly (*55*), together with our observation that oligomerized VDAC comes into close association with NLRP3, we examined whether mtDNA may play a role in NLRP3/VDAC aggregation. Depleting mtDNA did not block VDAC oligomerization but did block association of VDAC with NLRP3. Further, we found that transfecting mtDNA into the cytosol of cells depleted of mtDNA was not in itself sufficient to mobilized NLRP3 to bind VDAC or form an active NLRP3 inflammasome. However, although NLRP3-VDAC association was blocked in ATP-stimulated cells depleted of mtDNA, transfecting in mtDNA restored activation but only in the presence of ATP. This suggests a model in which VDAC plays two roles in NLRP3 inflammasome activation: First, it oligomerizes to form a pore large enough for mtDNA fragments to exit the mitochondria, and, second, it either binds to mtDNA, allowing for a bridge that links VDAC oligomers to NLRP3 aggregation and initiation of inflammasome assembly, or mtDNA binds to NLRP3 and stimulates its aggregation with VDAC and subsequent inflammasome activation.

Andreeva *et al.* (*74*) have proposed in a cryo–electron microscopy structure analysis of recombinant proteins that NLRP3 exists in a "12- to 16-mer double-ring cage" that is membrane localized [they suggest the trans-Golgi network (TGN)] that is disrupted by NEK7, leading to active inflammasome assembly (*74*). Similarly, Hochheiser *et al.* (*75*) suggested that the "inactive" form of NLRP3 is a decamer ring. In both cases, the "cage" formed is proposed to block pyrin domain interactions with downstream inflammasome components (*75*). We have not analyzed the multimeric structure

of the NLRP3 associating with oligomerized VDAC. It is possible that NLRP3 monomer binding to oligomerized VDAC facilitates assembly of larger NLRP3 oligomers on their way to becoming active. It is also possible that binding of preformed "caged" NLRP3 oligomers to oligomerized VDAC facilitates a structural shift that exposes NLRP3 pyrin domains for binding to ASC and further inflammasome assembly/activation.

We note that many of our experimental interventions are incomplete in their ability to block NLRP3 activation. It is possible that the interventions (e.g., inhibitor treatments) are incomplete and thus leave some remaining activity or that the interventions are completely effective but that another parallel pathway of NLRP3 activation exists that is unaffected. Our data are consistent with a large and growing body of work implicating mitochondria as a signaling nexus for NLRP3 inflammasome activation (*13*). However, additional studies have suggested that dissolution of the TGN and localization of NLRP3 to phosphatidylinositol 4-phosphate (PI4P) exposed on the dispersed vesicles facilitate NLRP3 inflammasome assembly (*67*, *76*). The vesicles are also thought to interact with mitochondria via PI4P (*77*). Thus, it is possible that the TGN-associated NLRP3 activation pathway is parallel to, downstream of, or upstream of the VDAC oligomerization requirement explored in this study and in Xian *et al.* (*21*).

HK2 has been widely studied as an antiapoptotic and mitochondria-stabilizing protein, often overexpressed in tumor cells, where it is thought to protect the cells from death (*78*). In this context, it is thought that interaction of HK with VDAC maintains VDAC in a "closed" state and prevents binding of proapoptotic Bcl family members Bax and Bid, which also interact with the same N-terminal tail of VDAC as HK2 (*30*, *34*, *40*, *46*, *56*, *79*, *80*). This relationship with regulation of cell death is intriguing, given that inflammasome activation often, but not always, is associated with an inflammatory type of cell death called pyroptosis. Thus, HK appears poised to influence the balance of multiple types of cell death and the inflammation that can result.

HK is fundamentally a metabolic enzyme, and yet we observe here that it is a nexus for inflammatory signaling in response to diverse stimuli and participates in setting up a cascade of events on the mitochondrial surface that promotes NLRP3 inflammasome activation. The events leading to initial aggregation of NLRP3 may be particularly attractive for designing strategies aimed at influencing the process, and the data here suggest novel approaches related to metabolic manipulations and targeting NLRP3 relocation across the mitochondrial surface. Healthy regulation of the NLRP3 inflammasome is important for diseases as wide-ranging as diabetes, obesity, atherosclerosis, and inflammatory bowel disease.

MATERIALS AND METHODS

Study design

The aim of the study was to identify how HK release from mitochondria leads to activation of the NLRP3 inflammasome. We used primary macrophages from wild-type and genetically modified mice. We used biochemical, genetic, and microscopy approaches to test a model of inflammasome activation in which HK release from the outer membrane led to changes in VDAC. All data were included, and no data or outliers were excluded. Sample size and experimental replicates are indicated in each figure caption. Unless otherwise stated, all n = values represent technical replicates, and, unless otherwise stated, all experiments were performed a minimum of three times with similar results. Investigators were not blinded to groups. The details of the reagents used are provided.

Animal experimental models

C57BL/6 mice and NLRP3$^{-/-}$ mice were purchased from the Jackson Laboratory. ASC$^{-/-}$ and control mice were provided by F. Sutterwala and S. Cassel. *Aim2*$^{-/-}$ mice were provided by C. Stehlik. Mice were housed under ad libitum access to food/water under specific pathogen–free conditions. Experimental cells were prepared from 6- to 12-week-old female C57BL/6 mice. For knockout experiments, cells were prepared from 6- to 25-week-old male and female mice with age- and sex-matched controls. All animal experimental procedures were conducted in accordance with Cedars-Sinai Medical Center Institutional Animal Care and Use Committee guidelines.

BMDM culture and stimulations

BMDMs were prepared as described previously with recombinant human macrophage colony-stimulating factor (M-CSF; 50 ng/ml; PeproTech, 300-25) (*12*). Cells were plated at 5.0 × 10^5 to 10.0 × 10^5/ml and primed with LPS (100 ng/ml; *Salmonella minnesota*, InvivoGen, tlrl-smlps) for 3 to 4 hours. For inflammasome activation and IL-1β measurements, primed BMDMs were treated by 2 to 5 mM ATP (MilliporeSigma, A2383) for 30 to 120 min, 3 to 10 μM nigericin (MilliporeSigma, 481990) for 30 to 120 min, N-terminal HK peptide or scramble peptide fused to transactivator of transcription peptide (HK-TAT and sc-TAT, respectively) [HK- MIASHLLAYFFTELN(β-Ala)GYGRKKRRQRRRG, sc-ATAFLMEYNSHLFIL(β-Ala)GYGRKKRRQRRRG] (United BioSystems) 20 μM for 2 hours, silica (20 to 100 μg/ml; MIN-U-SIL 15, U.S. Silica) for 6 hours, *Staphylococcus aureus* PGN (40 μg/ml; MilliporeSigma, 77140) for 6 hours, imiquimod (45 μg/ml; InvivoGen, tlrl-imq) for 90 min, or CL097 (45 μg/ml; InvivoGen, tlrl-c97-5) for 90 min. pdA:dT (InvivoGen, tlrl-patn) at 1 μg/ml in Opti-MEM (Gibco, 31985070) was mixed with Lipofectamine 2000 (Thermo Fisher Scientific, 11668019) for 30 min at room temperature and added at final concentration of 66 ng/ml to cells for 6 hours. Primed BMDMs were infected by *Salmonella typhimurium* (200 multiplicity of infection) for 30 min, and then the media were replaced with gentamicin-included media, followed by 2 hours of incubation. For noncanonical NLRP3 inflammasome activation, BMDMs were primed with Pam3CSK4 (1 μg/ml; InvivoGen, tlrl-pms) for 4 hours. Thirty minutes before stimulation, LPS (10 to 40 μg/ml) in Opti-MEM was prepared by mixing with FuGENE transfection reagent (Promega, E5911) and added at final concentration of 0.667 to 2.667 μg/ml to cells for 16 hours. For the inhibitor experiments, LPS-primed BMDMs were then pretreated for 1 hour with 20 μM VBIT-4 (Selleckchem, S3544), 100 μM 2-APB (Tocris Bioscience, 1224), 30 μM RuR (MilliporeSigma, 557450), and 20 μM CsA (MilliporeSigma, C3662), followed by addition of inflammasome activators as above.

CRISPR gRNA-Cas9 Neon transfection knockdown experiments

Short CRISPR RNAs (crRNAs) [VDAC1, CATCAACCTCGGCTGTGACG; VDAC2, GTGGAACACCGATAACACTC; VDAC3, ACACCAACTTATTGCGACCT; GRP75-1 (*Hspa9*-1), TTTGTTGCGGCACATTGTCA; GRP75-2 (*Hspa9*-2),

AAGACGCTTAGTAGCATAGA] were purchased from Integrated DNA Technologies (IDT). Duplex gRNAs were prepared by mixing equal amounts of 100 μM crRNAs and 100 μM trans-activating crRNA (tracrRNA) (IDT, 1072533) and heating at 95°C for 5 min. Transfection was performed with the Neon Transfection System (Thermo Fisher Scientific, MPK10096). The gRNAs were added into 100 μM Cas9 Electroporation Enhancer (IDT, 1075916) at a 3:1 molar ratio and mixed with 62 μM Alt-R Cas9 enzyme (IDT, 1081059) to make ribonucleoprotein (RNP) complex. A total of 2.0×10^6 of BMDMs resuspended in 100 μl of Neon buffer T were mixed with RNP complex and then electroporated at 1900 V, 20 ms, and 1 pulse. Cells were stimulated as above after 48 hours.

Enzyme-linked immunosorbent assay

Cell supernatants were used for enzyme-linked immunosorbent assay (ELISA) according to the manufacturer's instructions (IL-1β: BioLegend, 432601, and R&D Systems, DY401; IL-6 and TNF-α: Thermo Fisher Scientific, 88-7064-88 and 88-7324-88, respectively).

Lactate dehydrogenase assay

CytoTox 96 Non-Radioactive Cytotoxicity Assay (Promega, G1780) was used for measuring lactate dehydrogenase release following the manufacturer's instructions.

Cell fractionation and HK dissociation assays

Mitochondria were isolated by resuspending cells in 1.5 to 2 ml of ice-cold cell disruption buffer (20 mM Hepes, 10 mM KCl, 1.5 mM $MgCl_2$, 1 mM EDTA, and 250 mM sucrose, with fresh Sigma protease inhibitors). Cells were disrupted using nitrogen cavitation at 4°C for 5 min. Nuclei and cells were removed by centrifugation at 1000*g* for 5 min at 4°C. Mitochondria were isolated by centrifugation at 12,000*g* for 10 min at 4°C. Mitochondria were washed with cell disruption buffer and centrifuged at 9000*g* for 10 min at 4°C. The mitochondrion-enriched pellet was lysed in ice-cold radioimmunoprecipitation assay (RIPA) buffer [50 mM tris-HCl, 1% NP-40, 0.5% deoxycholate, 0.1% SDS, 150 mM NaCl, 2 mM EDTA, 50 mM NaF, and protease and phosphatase inhibitor cocktails (Sigma-Aldrich) (pH 7.4)]. Protein was quantitated using bicinchoninic acid (BCA) assay Protein Assay (Pierce, 23227). In some cases, cytosol was isolated by adding digitonin (50 μg/ml) to the cell disruption buffer and incubating with rocking for 10 min. Lysates were centrifuged at 10,000*g* for 10 min, and supernatants were designated cytosol. If necessary, cytosol was concentrated using Amicon 0.5-ml 3-kDa concentrators (Millipore). Protein was quantified using BCA Protein Assay or Coomassie Protein Assay (Thermo Fisher Scientific, 23236). Cytosol was mixed with Laemmli sample buffer with β-mercaptoethanol, boiled at 95°C for 10 min, and subject to immunoblotting.

Immunoblots and VDAC cross-linking assay

Lysates were prepared with NuPAGE LDS sample buffer (Thermo Fisher Scientific, NP0008) containing β-mercaptoethanol. For supernatants, cells were treated with serum-free Opti-MEM medium. Supernatants for IL-1β were precipitated using Strata-Clean Resin (Agilent Technologies, 400714) and resuspended in Laemmli sample buffer (Bio-Rad, 1610747). Samples were boiled at 95°C for 10 min. For cross-linking assay, cells (1 mg/ml) in Dulbecco's phosphate-buffered saline (DPBS) (pH 8.3) were incubated with 200 μM ethylene glycol bis(succinimidyl succinate) (Thermo Fisher Scientific, 21565) at 30°C for 15 min. After adding LDS sample buffer, samples were boiled at 70°C for 10 min and sonicated for 10 s twice. Samples were resolved on 4 to 12% polyacrylamide bis-tris gels (Thermo Fisher Scientific) and transferred to polyvinylidene difluoride membranes (Merck Millipore) using a Trans-Blot Turbo Transfer System (Bio-Rad). Membranes were incubated at 4°C overnight with the following primary antibodies as indicated: VDAC1/Porin [1:1,000 unless otherwise stated; EPR10852(B), Abcam, ab154856], VDAC3 (1:1000; MilliporeSigma, SAB2108497), IL-1β (1:1000; R&D Systems, AF-401-NA), caspase-1 p10 (1:1000; Santa Cruz Biotechnology, sc-514), β-tubulin (1:1000; TUB 2.1, MilliporeSigma, T-4026), HK2 (1:1000; C64G5, Cell Signaling Technology, 2867), HK1 (1:1000; G-1, Santa Cruz Biotechnology, sc-46695), cytochrome *c* (1:500; A-8, Santa Cruz Biotechnology, sc-13156), glyceraldehyde-3-phosphate dehydrogenase (GAPDH; 1:1000; 6C5, Santa Cruz Biotechnology, sc-32233), VDAC 1/2/3 (used for Figs. 1C, 6M, and 7G only) (1:1000; D73D12, Cell Signaling Technology, 4661), ASC (1:1000; Enzo, ADI-905-173-100), or NLRP3/NALP3 (1:1000; Cryo-2, AdipoGen, 102514-284) and then at room temperature for 1 hour with secondary antibodies coupled to either infrared dye (1:15,000; Biotium or LI-COR) or horseradish peroxidase (HRP; 1:5000; Jackson Immunobiology). HRP secondaries were detected with ECL Pico Plus (Thermo Fisher Scientific). Immunoblots were imaged using Odyssey (LI-COR), Chemidoc (Bio-Rad), or film. Dimers, trimers, and multimers of VDAC1 were quantified using Image Lab software (Bio-Rad).

Cytochemistry and proximity ligation assay

Cells were plated on 12-mm round coverslips as described (*12*). Cells treated as indicated were rinsed with warmed DPBS and fixed with 4% paraformaldehyde for 15 min. Guanidine hydrochloride or tris buffer (6 M; pH 10.0; Abcam) was used to retrieve antigen for 10 min at room temperature or 95°C, respectively. For permeabilizing and blocking, cells were treated with 0.1% Triton X-100 for 10 min, followed by 1% bovine serum albumin (BSA) and glycine (22.52 mg/ml) in PBS with 0.1% Tween 20 for 40 min. Cells were incubated at 4°C overnight with following primary antibodies as indicated: VDAC1/Porin [1:100; EPR10852(B), Abcam, ab154856], HK2 (1:100; OTI4C5, Bio-Rad, VMA00174), or NLRP3/NALP3 (1:100; Cryo-2, AdipoGen, 102514-284). Cells were incubated at room temperature for 1 hour with Alexa Fluor 488– or Alexa Fluor 594–conjugated immunoglobulin G (1:100; Thermo Fisher Scientific). ProLong Gold Antifade Mountant (Thermo Fisher Scientific) was used for mounting.

For proximity ligation assay (PLA), fixed and permeabilized cells were blocked as described above and stained with VDAC1/Porin [1:100; EPR10852(B), Abcam, ab154856] and NLRP3/NALP3 (1:100; Cryo-2, AdipoGen, 102514-284). PLA was performed using Duolink In Situ PLA Kit (MilliporeSigma, DUO92008 and DUO92014) following the manufacturer's instructions. PLA results were quantified by two approaches using ImageJ software. Integrated signal density was measured in individual cells and reported as "PLA signal/cell [relative fluorescence units (RFU)]" or as fold change compared with untreated control samples. Alternatively, PLA signal per field of view was measured normalized to 4′,6-diamidino-2-phenylindole (DAPI) signal per field and reported as

fold change compared with control samples and labeled "normalized PLA signal/field (fold)."

τ-STED–FLIM imaging and acceptor photobleaching assay

A Stellaris 8 STED microscope (Leica) with a HC Plan-Apochromat CS2 100×/1.4 oil-immersion objective lens was used for τ-STED imaging and FLIM τ-STED imaging. The laser was aligned at 80% of power, and the pixel size was set to 18.94 nm. *Z*-stack images were acquired with a 0.3-μm interval. The volume of each VDAC1 cluster for a single mitochondrion was measured and then averaged. Each dot represents the average volume of each VDAC1 cluster in a single mitochondrion. VDAC1 cluster volume was measured using Imaris software (Bitplane). For acceptor photobleaching assays, regions of interest were randomly designated, and acceptor photobleaching was performed using a Stellaris 8 STED microscope. The efficiency of donor fluorescence in photobleached areas was measured using Leica Application Suite X software (Leica). Images showing colocalization of VDAC1 and NLRP3 were extracted using the "RG2B colocalization" plugin of ImageJ. Integrated density of colocalized signals was normalized by integrated density of VDAC1 signals of each cell.

Caspase-1 activity assay

Caspase-Glo 1 Inflammasome Assay kit (Promega, G9951) was used for measuring the activity of caspase-1 following the manufacturer's instructions.

GFP-HK2 expression and live cell imaging

All GFP-HK2 transduction of BMDMs and live cell imaging were performed as described previously (*12*).

Quantitative polymerase chain reaction

RNA was extracted from cells using the RNeasy kit (QIAGEN) or DNA using the QiaAMP kit (QIAGEN) according to the manufacturer's instructions. Gene expression was determined using SYBR Green (Bio-Rad) with gene specific primers (IDT). PrimeTime qPCR primer sets were as follows: Vdac1, Mm.PT.58.43905165; Vdac2, Mm.PT.58.30492179; Vdac3, Mm.PT.58.5914193; Hprt, AGGTTGCAAGCTTGCTGGT (forward) and TGAAGTACTCATTATAGTCAAGG (reverse); D loop, CCCAAGCATATAAGCTAGTAC (forward) and ATATAAGTCATATTTTGGGGAACTAC (reverse); CoxI, CCAGTGCTAGCCGCAGGCAT (S598) and TTGGGTCCCCTCCTCCAGCGG (AS685); Gapdh, GGTCTACATGTTCCAGTATGACT (forward) and GGGTCTCGCTCCTGGAAGAT (reverse). Data were collected on a qTOWER (Analytica Gena), analyzed by $2^{-\Delta Ct}$, normalized to a housekeeping gene, and plotted as fold induction.

Mitochondrial calcium measurement

BMDMs were primed with LPS for 3 hours, washed with Hanks' balanced salt solution (HBSS) containing 25 mM glucose and 0.5% BSA once, and stained with a final concentration of 5 μM Rhod-2 AM (Thermo Fisher Scientific, R1245MP) in 0.04% F127 Pluronic (Thermo Fisher Scientific, P2443) in HBSS solution for 20 min at 37°C. Cells were washed three times with phenol red–free RPMI 1640 culture medium and stabilized for 30 min at 37°C. Cells were treated as indicated, and Rhod-2 AM fluorescence was read by a CLARIOstar plate reader.

mtDNA depletion, isolation, and transfer

For mtDNA depletion, BMDMs were treated with culture media containing M-CSF and EtBr (900 ng/ml), and it was replaced every 2 days for 2 weeks (*21*, *22*, *71*). mtDNA was quantified by SYBR Green (Bio-Rad, 1725272) qPCR using D loop (forward, CCCAAGCATATAAGCAAGTAC; reverse, GTAGTTCCCAAAATATGACTTATAT) and CoxI (forward, TTCGGAGCCTGAGCGGGAAT; reverse, ATGCCTGCGGCTAGCACTGG) on a qTOWER qPCR machine (Analytik Jena) (*12*). Mitochondria from BMDMs were isolated for immunoblotting and mtDNA isolation for transfection nitrogen cavitation to disrupt the plasma membrane and centrifugation to purify the mitochondria (*81*), followed by lysis in RIPA buffer or mtDNA isolation using the QIAamp DNA Mini Kit (QIAGEN, 51304). Isolated mtDNA was dissolved in water and stored at −20°C. mtDNA (3 μg/ml) in Opti-MEM was prepared by mixing with Lipofectamine 2000 for 30 min at room temperature and added to LPS-primed BMDMs for 5 hours, followed by ATP treatment at final concentration of 2 mM for 1 hour.

Human blood-derived monocyte isolation and stimulation

Blood was collected from male and female healthy donors after informed consent by the Cedars-Sinai Medical Center MIRIAD Biobank in accordance with Cedars-Sinai Medical Center Institutional Review Board procedures. Peripheral blood mononuclear cells were separated using Ficoll-Paque (Cytiva). Monocytes were isolated using the MojoSort Human CD14 Selection Kit (BioLegend, 480026) and an autoMACS Pro Separator (Miltenyi). Monocytes were stimulated with 2 μg/ml for 24 hours. IL-1β was measured by ELISA (BioLegend, 437004).

Statistical analysis

GraphPad Prism 8.0 software or Excel was used for data analysis. Data are presented as means ± SEM. Statistical significance was determined by *t* tests (two-tailed) or one-way or two-way analysis of variance (ANOVA) with multiple comparisons test for more groups. $P < 0.05$ was considered statistically significant where $^{*}P < 0.05$, $^{**}P < 0.01$, $^{***}P < 0.001$, and $^{****}P < 0.0001$.

Supplementary Materials

This PDF file includes:
Figs. S1 to S6

Other Supplementary Material for this manuscript includes the following:
Data file S1
MDAR Reproducibility Checklist

View/request a protocol for this paper from *Bio-protocol*.

REFERENCES AND NOTES

1. K. Nozaki, L. Li, E. A. Miao, Innate sensors trigger regulated cell death to combat intracellular infection. *Annu. Rev. Immunol.* **40**, 469–498 (2022).
2. S. Tartey, T. D. Kanneganti, Differential role of the NLRP3 inflammasome in infection and tumorigenesis. *Immunology* **156**, 329–338 (2019).
3. R. Grant, V. Dixit, Mechanisms of disease: Inflammasome activation and the development of type 2 diabetes. *Front. Immunol.* **4**, 50 (2013).
4. T.-C. Tzeng, D. Golenbock, NLRP3 inflammasome activation in Alzheimer's disease (INC9P.446). *J. Immunol.* **192**, 188.5 (2014).

5. Y. Zhang, Z. Dong, W. Song, NLRP3 inflammasome as a novel therapeutic target for Alzheimer's disease. *Signal Transduct. Target. Ther.* **5**, 37 (2020).
6. T. van der Heijden, E. Kritikou, W. Venema, J. van Duijn, P. J. van Santbrink, B. Slütter, A. C. Foks, I. Bot, J. Kuiper, NLRP3 inflammasome inhibition by MCC950 reduces atherosclerotic lesion development in apolipoprotein E-deficient mice-brief report. *Arterioscler. Thromb. Vasc. Biol.* **37**, 1457–1461 (2017).
7. I. C. Allen, E. M. TeKippe, R.-M. T. Woodford, J. M. Uronis, E. K. Holl, A. B. Rogers, H. H. Herfarth, C. Jobin, J. P.-Y. Ting, The NLRP3 inflammasome functions as a negative regulator of tumorigenesis during colitis-associated cancer. *J. Exp. Med.* **207**, 1045–1056 (2010).
8. C. Bauer, P. Duewell, C. Mayer, H. A. Lehr, K. A. Fitzgerald, M. Dauer, J. Tschopp, S. Endres, E. Latz, M. Schnurr, Colitis induced in mice with dextran sulfate sodium (DSS) is mediated by the NLRP3 inflammasome. *Gut* **59**, 1192–1199 (2010).
9. A. P. Perera, R. Fernando, T. Shinde, R. Gundamaraju, B. Southam, S. S. Sohal, A. A. B. Robertson, K. Schroder, D. Kunde, R. Eri, MCC950, a specific small molecule inhibitor of NLRP3 inflammasome attenuates colonic inflammation in spontaneous colitis mice. *Sci. Rep.* **8**, 8618 (2018).
10. Y. Zhen, H. Zhang, NLRP3 inflammasome and inflammatory bowel disease. *Front. Immunol.* **10**, 276 (2019).
11. T. Shimada, B. G. Park, A. J. Wolf, C. Brikos, H. S. Goodridge, C. A. Becker, C. N. Reyes, E. A. Miao, A. Aderem, F. Gotz, G. Y. Liu, D. M. Underhill, *Staphylococcus aureus* evades lysozyme-based peptidoglycan digestion that links phagocytosis, inflammasome activation, and IL-1β secretion. *Cell Host Microbe* **7**, 38–49 (2010).
12. A. J. Wolf, C. N. Reyes, W. Liang, C. Becker, K. Shimada, M. L. Wheeler, H. C. Cho, N. I. Popescu, K. M. Coggeshall, M. Arditi, D. M. Underhill, Hexokinase is an innate immune receptor for the detection of bacterial peptidoglycan. *Cell* **166**, 624–636 (2016).
13. K. V. Swanson, M. Deng, J. P. Ting, The NLRP3 inflammasome: Molecular activation and regulation to therapeutics. *Nat. Rev. Immunol.* **19**, 477–489 (2019).
14. C. J. Gross, R. Mishra, K. S. Schneider, G. Medard, J. Wettmarshausen, D. C. Dittlein, H. Shi, O. Gorka, P. A. Koenig, S. Fromm, G. Magnani, T. Cikovic, L. Hartjes, J. Smollich, A. A. B. Robertson, M. A. Cooper, M. Schmidt-Supprian, M. Schuster, K. Schroder, P. Broz, C. Traidl-Hoffmann, B. Beutler, B. Kuster, J. Ruland, S. Schneider, F. Perocchi, O. Gross, K^+ efflux-independent NLRP3 inflammasome activation by small molecules targeting mitochondria. *Immunity* **45**, 761–773 (2016).
15. M. M. Gaidt, T. S. Ebert, D. Chauhan, T. Schmidt, J. L. Schmid-Burgk, F. Rapino, A. A. Robertson, M. A. Cooper, T. Graf, V. Hornung, Human monocytes engage an alternative inflammasome pathway. *Immunity* **44**, 833–846 (2016).
16. M. Karmakar, M. Minns, E. N. Greenberg, J. Diaz-Aponte, K. Pestonjamasp, J. L. Johnson, J. K. Rathkey, D. W. Abbott, K. Wang, F. Shao, S. D. Catz, G. R. Dubyak, E. Pearlman, N-GSDMD trafficking to neutrophil organelles facilitates IL-1β release independently of plasma membrane pores and pyroptosis. *Nat. Commun.* **11**, 2212 (2020).
17. T. Murakami, J. Ockinger, J. Yu, V. Byles, A. McColl, A. M. Hofer, T. Horng, Critical role for calcium mobilization in activation of the NLRP3 inflammasome. *Proc. Natl. Acad. Sci. U.S.A.* **109**, 11282–11287 (2012).
18. R. Zhou, A. S. Yazdi, P. Menu, J. Tschopp, A role for mitochondria in NLRP3 inflammasome activation. *Nature* **469**, 221–225 (2011).
19. K. Shimada, T. R. Crother, J. Karlin, J. Dagvadorj, N. Chiba, S. Chen, V. K. Ramanujan, A. J. Wolf, L. Vergnes, D. M. Ojcius, A. Rentsendorj, M. Vargas, C. Guerrero, Y. Wang, K. A. Fitzgerald, D. M. Underhill, T. Town, M. Arditi, Oxidized mitochondrial DNA activates the NLRP3 inflammasome during apoptosis. *Immunity* **36**, 401–414 (2012).
20. G. Tumurkhuu, K. Shimada, J. Dagvadorj, T. R. Crother, W. Zhang, D. Luthringer, R. A. Gottlieb, S. Chen, M. Arditi, Ogg1-dependent DNA repair regulates NLRP3 inflammasome and prevents atherosclerosis. *Circ. Res.* **119**, e76–e90 (2016).
21. H. Xian, K. Watari, E. Sanchez-Lopez, J. Offenberger, J. Onyuru, H. Sampath, W. Ying, H. M. Hoffman, G. S. Shadel, M. Karin, Oxidized DNA fragments exit mitochondria via mPTP- and VDAC-dependent channels to activate NLRP3 inflammasome and interferon signaling. *Immunity* **55**, 1370–1385.e8 (2022).
22. Z. Zhong, S. Liang, E. Sanchez-Lopez, F. He, S. Shalapour, X.-j. Lin, J. Wong, S. Ding, E. Seki, B. Schnabl, A. L. Hevener, H. B. Greenberg, T. Kisseleva, M. Karin, New mitochondrial DNA synthesis enables NLRP3 inflammasome activation. *Nature* **560**, 198–203 (2018).
23. E. I. Elliott, A. N. Miller, B. Banoth, S. S. Iyer, A. Stotland, J. P. Weiss, R. A. Gottlieb, F. S. Sutterwala, S. L. Cassel, Cutting edge: Mitochondrial assembly of the NLRP3 inflammasome complex is initiated at priming. *J. Immunol.* **200**, 3047–3052 (2018).
24. S. S. Iyer, Q. He, J. R. Janczy, E. I. Elliott, Z. Zhong, A. K. Olivier, J. J. Sadler, V. Knepper-Adrian, R. Han, L. Qiao, S. C. Eisenbarth, W. M. Nauseef, S. L. Cassel, F. S. Sutterwala, Mitochondrial cardiolipin is required for Nlrp3 inflammasome activation. *Immunity* **39**, 311–323 (2013).
25. J. Liu, T. Wang, K. He, M. Xu, J. P. Gong, Cardiolipin inhibitor ameliorates the non-alcoholic steatohepatitis through suppressing NLRP3 inflammasome activation. *Eur. Rev. Med. Pharmacol. Sci.* **23**, 8158–8167 (2019).
26. S. Park, C. Juliana, S. Hong, P. Datta, I. Hwang, T. Fernandes-Alnemri, J. W. Yu, E. S. Alnemri, The mitochondrial antiviral protein MAVS associates with NLRP3 and regulates its inflammasome activity. *J. Immunol.* **191**, 4358–4366 (2013).
27. N. Subramanian, K. Natarajan, M. R. Clatworthy, Z. Wang, R. N. Germain, The adaptor MAVS promotes NLRP3 mitochondrial localization and inflammasome activation. *Cell* **153**, 348–361 (2013).
28. P. I. Seoane, B. Lee, C. Hoyle, S. Yu, G. Lopez-Castejon, M. Lowe, D. Brough, The NLRP3–I-nflammasome as a sensor of organelle dysfunction. *J. Cell Biol.* **219**, (2020).
29. S. Alfonso-Loeches, J. R. Urena-Peralta, M. J. Morillo-Bargues, J. Oliver-De La Cruz, C. Guerri, Role of mitochondria ROS generation in ethanol-induced NLRP3 inflammasome activation and cell death in astroglial cells. *Front. Cell. Neurosci.* **8**, 216 (2014).
30. A. Klepinin, L. Ounpuu, K. Mado, L. Truu, V. Chekulayev, M. Puurand, I. Shevchuk, K. Tepp, A. Planken, T. Kaambre, The complexity of mitochondrial outer membrane permeability and VDAC regulation by associated proteins. *J. Bioenerg. Biomembr.* **50**, 339–354 (2018).
31. D. J. Roberts, S. Miyamoto, Hexokinase II integrates energy metabolism and cellular protection: Akting on mitochondria and TORCing to autophagy. *Cell Death Differ.* **22**, 248–257 (2015).
32. S. John, J. N. Weiss, B. Ribalet, Subcellular localization of hexokinases I and II directs the metabolic fate of glucose. *PLOS ONE* **6**, e17674 (2011).
33. A. De Jesus, F. Keyhani-Nejad, C. M. Pusec, L. Goodman, J. A. Geier, J. S. Stoolman, P. J. Stanczyk, T. Nguyen, K. Xu, K. V. Suresh, Y. Chen, A. E. Rodriguez, J. S. Shapiro, H. C. Chang, C. Chen, K. P. Shah, I. Ben-Sahra, B. T. Layden, N. S. Chandel, S. E. Weinberg, H. Ardehali, Hexokinase 1 cellular localization regulates the metabolic fate of glucose. *Mol. Cell* **82**, 1261–1277.e9 (2022).
34. A. K. S. Camara, Y. Zhou, P. C. Wen, E. Tajkhorshid, W. M. Kwok, Mitochondrial VDAC1: A key gatekeeper as potential therapeutic target. *Front. Physiol.* **8**, 460 (2017).
35. S. Abu-Hamad, N. Arbel, D. Calo, L. Arzoine, A. Israelson, N. Keinan, R. Ben-Romano, O. Friedman, V. Shoshan-Barmatz, The VDAC1 N-terminus is essential both for apoptosis and the protective effect of anti-apoptotic proteins. *J. Cell Sci.* **122**, 1906–1916 (2009).
36. V. Betaneli, E. P. Petrov, P. Schwille, The role of lipids in VDAC oligomerization. *Biophys. J.* **102**, 523–531 (2012).
37. N. Keinan, D. Tyomkin, V. Shoshan-Barmatz, Oligomerization of the mitochondrial protein voltage-dependent anion channel is coupled to the induction of apoptosis. *Mol. Cell. Biol.* **30**, 5698–5709 (2010).
38. J. T. Varughese, S. K. Buchanan, A. S. Pitt, The role of voltage-dependent anion channel in mitochondrial dysfunction and human disease. *Cell* **10**, (2021).
39. R. Zalk, A. Israelson, E. S. Garty, H. Azoulay-Zohar, V. Shoshan-Barmatz, Oligomeric states of the voltage-dependent anion channel and cytochrome c release from mitochondria. *Biochem. J.* **386**, 73–83 (2005).
40. Y. Tsujimoto, S. Shimizu, VDAC regulation by the Bcl-2 family of proteins. *Cell Death Differ.* **7**, 1174–1181 (2000).
41. F. Ciscato, R. Filadi, I. Masgras, M. Pizzi, O. Marin, N. Damiano, P. Pizzo, A. Gori, F. Frezzato, F. Chiara, L. Trentin, P. Bernardi, A. Rasola, Hexokinase 2 displacement from mitochondria-associated membranes prompts Ca^{2+} –dependent death of cancer cells. *EMBO Rep.* **21**, e49117 (2020).
42. R. Muñoz-Planillo, P. Kuffa, G. Martínez-Colón, B. L. Smith, T. M. Rajendiran, G. Núñez, K^+ efflux is the common trigger of NLRP3 inflammasome activation by bacterial toxins and particulate matter. *Immunity* **38**, 1142–1153 (2013).
43. V. Pétrilli, S. Papin, C. Dostert, A. Mayor, F. Martinon, J. Tschopp, Activation of the NALP3 inflammasome is triggered by low intracellular potassium concentration. *Cell Death Differ.* **14**, 1583–1589 (2007).
44. A. Tapia-Abellán, D. Angosto-Bazarra, C. Alarcón-Vila, M. C. Baños, I. Hafner-Bratkovi˘, B. Oliva, P. Pelegrín, Sensing low intracellular potassium by NLRP3 results in a stable open structure that promotes inflammasome activation. *Sci. Adv.* **7**, eabf4468 (2021).
45. J. G. Pastorino, J. B. Hoek, Regulation of hexokinase binding to VDAC. *J. Bioenerg. Biomembr.* **40**, 171–182 (2008).
46. L. Arzoine, N. Zilberberg, R. Ben-Romano, V. Shoshan-Barmatz, Voltage-dependent anion channel 1-based peptides interact with hexokinase to prevent its anti-apoptotic activity. *J. Biol. Chem.* **284**, 3946–3955 (2009).
47. V. Shoshan-Barmatz, A. Shteinfer-Kuzmine, A. Verma, VDAC1 at the intersection of cell metabolism, apoptosis, and diseases. *Biomolecules* **10**, (2020).
48. N. Keinan, H. Pahima, D. Ben-Hail, V. Shoshan-Barmatz, The role of calcium in VDAC1 oligomerization and mitochondria-mediated apoptosis. *Biochim. Biophys. Acta* **1833**, 1745–1754 (2013).
49. A. Israelson, H. Zaid, S. Abu-Hamad, E. Nahon, V. Shoshan-Barmatz, Mapping the ruthenium red-binding site of the voltage-dependent anion channel-1. *Cell Calcium* **43**, 196–204 (2008).

50. V. P. Tan, J. M. Smith, M. Tu, J. D. Yu, E. Y. Ding, S. Miyamoto, Dissociation of mitochondrial HK-II elicits mitophagy and confers cardioprotection against ischemia. *Cell Death Dis.* **10**, 730 (2019).
51. F. Chiara, D. Castellaro, O. Marin, V. Petronilli, W. S. Brusilow, M. Juhaszova, S. J. Sollott, M. Forte, P. Bernardi, A. Rasola, Hexokinase II detachment from mitochondria triggers apoptosis through the permeability transition pore independent of voltage-dependent anion channels. *PLOS ONE* **3**, e1852 (2008).
52. S. Weisthal, N. Keinan, D. Ben-Hail, T. Arif, V. Shoshan-Barmatz, Ca^{2+}-mediated regulation of VDAC1 expression levels is associated with cell death induction. *Biochim. Biophys. Acta* **1843**, 2270–2281 (2014).
53. D. Ben-Hail, R. Begas-Shvartz, M. Shalev, A. Shteinfer-Kuzmine, A. Gruzman, S. Reina, V. De Pinto, V. Shoshan-Barmatz, Novel compounds targeting the mitochondrial protein VDAC1 inhibit apoptosis and protect against mitochondrial dysfunction. *J. Biol. Chem.* **291**, 24986–25003 (2016).
54. A. Verma, S. Pittala, B. Alhozeel, A. Shteinfer-Kuzmine, E. Ohana, R. Gupta, J. H. Chung, V. Shoshan-Barmatz, The role of the mitochondrial protein VDAC1 in inflammatory bowel disease: A potential therapeutic target. *Mol. Ther.* **30**, 726–744 (2022).
55. J. Kim, R. Gupta, L. P. Blanco, S. Yang, A. Shteinfer-Kuzmine, K. Wang, J. Zhu, H. E. Yoon, X. Wang, M. Kerkhofs, H. Kang, A. L. Brown, S.-J. Park, X. Xu, E. Zandee van Rilland, M. K. Kim, J. I. Cohen, M. J. Kaplan, V. Shoshan-Barmatz, J. H. Chung, VDAC oligomers form mitochondrial pores to release mtDNA fragments and promote lupus-like disease. *Science* **366**, 1531–1536 (2019).
56. Y. Zheng, Y. Shi, C. Tian, C. Jiang, H. Jin, J. Chen, A. Almasan, H. Tang, Q. Chen, Essential role of the voltage-dependent anion channel (VDAC) in mitochondrial permeability transition pore opening and cytochrome c release induced by arsenic trioxide. *Oncogene* **23**, 1239–1247 (2004).
57. A. Messina, S. Reina, F. Guarino, V. De Pinto, VDAC isoforms in mammals. *Biochim. Biophys. Acta* **1818**, 1466–1476 (2012).
58. C. Bryant, Inflammasome activation by *salmonella*. *Curr. Opin. Microbiol.* **64**, 27–32 (2021).
59. J. H. Bae, J. W. Park, T. K. Kwon, Ruthenium red, inhibitor of mitochondrial Ca^{2+} uniporter, inhibits curcumin-induced apoptosis via the prevention of intracellular Ca^{2+} depletion and cytochrome c release. *Biochem. Biophys. Res. Commun.* **303**, 1073–1079 (2003).
60. J. J. Woods, J. J. Wilson, Inhibitors of the mitochondrial calcium uniporter for the treatment of disease. *Curr. Opin. Chem. Biol.* **55**, 9–18 (2020).
61. D. Gincel, H. Zaid, V. Shoshan-Barmatz, Calcium binding and translocation by the voltage-dependent anion channel: A possible regulatory mechanism in mitochondrial function. *Biochem. J.* **358**, 147–155 (2001).
62. G. Amanakis, E. Murphy, Cyclophilin D: An integrator of mitochondrial function. *Front. Physiol.* **11**, 595 (2020).
63. Y. Liu, X. Ma, H. Fujioka, J. Liu, S. Chen, X. Zhu, DJ-1 regulates the integrity and function of ER-mitochondria association through interaction with IP3R3-Grp75-VDAC1. *Proc. Natl. Acad. Sci. U.S.A.* **116**, 25322–25328 (2019).
64. G. Szabadkai, K. Bianchi, P. Varnai, D. De Stefani, M. R. Wieckowski, D. Cavagna, A. I. Nagy, T. Balla, R. Rizzuto, Chaperone-mediated coupling of endoplasmic reticulum and mitochondrial Ca^{2+} channels. *J. Cell Biol.* **175**, 901–911 (2006).
65. J. A. Hagar, D. A. Powell, Y. Aachoui, R. K. Ernst, E. A. Miao, Cytoplasmic LPS activates caspase-11: Implications in TLR4-independent endotoxic shock. *Science* **341**, 1250–1253 (2013).
66. N. Kayagaki, M. T. Wong, I. B. Stowe, S. R. Ramani, L. C. Gonzalez, S. Akashi-Takamura, K. Miyake, J. Zhang, W. P. Lee, A. Muszynski, L. S. Forsberg, R. W. Carlson, V. M. Dixit, Noncanonical inflammasome activation by intracellular LPS independent of TLR4. *Science* **341**, 1246–1249 (2013).
67. J. Chen, Z. J. Chen, PtdIns4P on dispersed trans-Golgi network mediates NLRP3 inflammasome activation. *Nature* **564**, 71–76 (2018).
68. T. Misawa, M. Takahama, T. Kozaki, H. Lee, J. Zou, T. Saitoh, S. Akira, Microtubule-driven spatial arrangement of mitochondria promotes activation of the NLRP3 inflammasome. *Nat. Immunol.* **14**, 454–460 (2013).
69. C. S. Yang, J. J. Kim, T. S. Kim, P. Y. Lee, S. Y. Kim, H. M. Lee, D. M. Shin, L. T. Nguyen, M. S. Lee, H. S. Jin, K. K. Kim, C. H. Lee, M. H. Kim, S. G. Park, J. M. Kim, H. S. Choi, E. K. Jo, Small heterodimer partner interacts with NLRP3 and negatively regulates activation of the NLRP3 inflammasome. *Nat. Commun.* **6**, 6115 (2015).
70. Y. Qiu, Y. Huang, M. Chen, Y. Yang, X. Li, W. Zhang, Mitochondrial DNA in NLRP3 inflammasome activation. *Int. Immunopharmacol.* **108**, 108719 (2022).
71. E. B. Warren, A. E. Aicher, J. P. Fessel, C. Konradi, Mitochondrial DNA depletion by ethidium bromide decreases neuronal mitochondrial creatine kinase: Implications for striatal energy metabolism. *PLOS ONE* **12**, e0190456 (2017).
72. V. A. K. Rathinam, Y. Zhao, F. Shao, Innate immunity to intracellular LPS. *Nat. Immunol.* **20**, 527–533 (2019).
73. M. Bonora, C. Giorgi, P. Pinton, Molecular mechanisms and consequences of mitochondrial permeability transition. *Nat. Rev. Mol. Cell Biol.* **23**, 266–285 (2022).
74. L. Andreeva, L. David, S. Rawson, C. Shen, T. Pasricha, P. Pelegrin, H. Wu, NLRP3 cages revealed by full-length mouse NLRP3 structure control pathway activation. *Cell* **184**, 6299–6312.e22 (2021).
75. I. V. Hochheiser, M. Pilsl, G. Hagelueken, J. Moecking, M. Marleaux, R. Brinkschulte, E. Latz, C. Engel, M. Geyer, Structure of the NLRP3 decamer bound to the cytokine release inhibitor CRID3. *Nature* **604**, 184–189 (2022).
76. N. A. Schmacke, F. O'Duill, M. M. Gaidt, I. Szymanska, J. M. Kamper, J. L. Schmid-Burgk, S. C. Madler, T. Mackens-Kiani, T. Kozaki, D. Chauhan, D. Nagl, C. A. Stafford, H. Harz, A. L. Frohlich, F. Pinci, F. Ginhoux, R. Beckmann, M. Mann, H. Leonhardt, V. Hornung, IKKβ primes inflammasome formation by recruiting NLRP3 to the trans-Golgi network. *Immunity* **55**, 2271–2284.e7 (2022).
77. L. C. Tabara, J. L. Morris, J. Prudent, The complex dance of organelles during mitochondrial division. *Trends Cell Biol.* **31**, 241–253 (2021).
78. F. Ciscato, L. Ferrone, I. Masgras, C. Laquatra, A. Rasola, Hexokinase 2 in cancer: A prima donna playing multiple characters. *Int. J. Mol. Sci.* **22**, (2021).
79. J. Lauterwasser, F. Todt, R. M. Zerbes, T. N. Nguyen, W. Craigen, M. Lazarou, M. van der Laan, F. Edlich, The porin VDAC2 is the mitochondrial platform for Bax retrotranslocation. *Sci. Rep.* **6**, 32994 (2016).
80. T. K. Rostovtseva, S. M. Bezrukov, D. P. Hoogerheide, Regulation of mitochondrial respiration by VDAC is enhanced by membrane-bound inhibitors with disordered polyanionic C-terminal domains. *Int. J. Mol. Sci.* **22**, 7358 (2021).
81. R. A. Gottlieb, S. Adachi, Nitrogen cavitation for cell disruption to obtain mitochondria from cultured cells. *Methods Enzymol.* **322**, 213–221 (2000).

Acknowledgments

Funding: This study was supported by National Institutes of Health grants R01 AI148465 (to A.J.W.), R01 GM085796 (to D.M.U.), and R01 AI071116 (to D.M.U.). **Author contributions:** Conceptualization: S.H.B., A.J.W., and D.M.U. Methodology: S.H.B., A.J.W., and V.K.R. Investigation: S.H.B., A.J.W., C.B., and S.F. Visualization: S.H.B. and A.J.W. Funding acquisition: A.J.W. and D.M.U. Project administration: A.J.W. and D.M.U. Supervision A.J.W. and D.M.U. Writing—original draft: S.H.B., A.J.W., and D.M.U. Writing—review and editing: S.H.B., A.J.W., and D.M.U. **Competing interests:** The authors declare that they have no competing interests. **Data and materials availability:** All data needed to support the conclusions of the paper are available in the main text or the Supplementary Materials. Materials are available upon request from the corresponding authors.

Submitted 6 September 2022
Accepted 25 May 2023
Published 16 June 2023
10.1126/sciimmunol.ade7652